Advances in Quantitative MRI: Acquisition, Estimation, and Application

Gopal Nataraj

Dissertation Defense
March 23, 2018

Dept. of Electrical Engineering and Computer Science
University of Michigan

Example: flow imaging

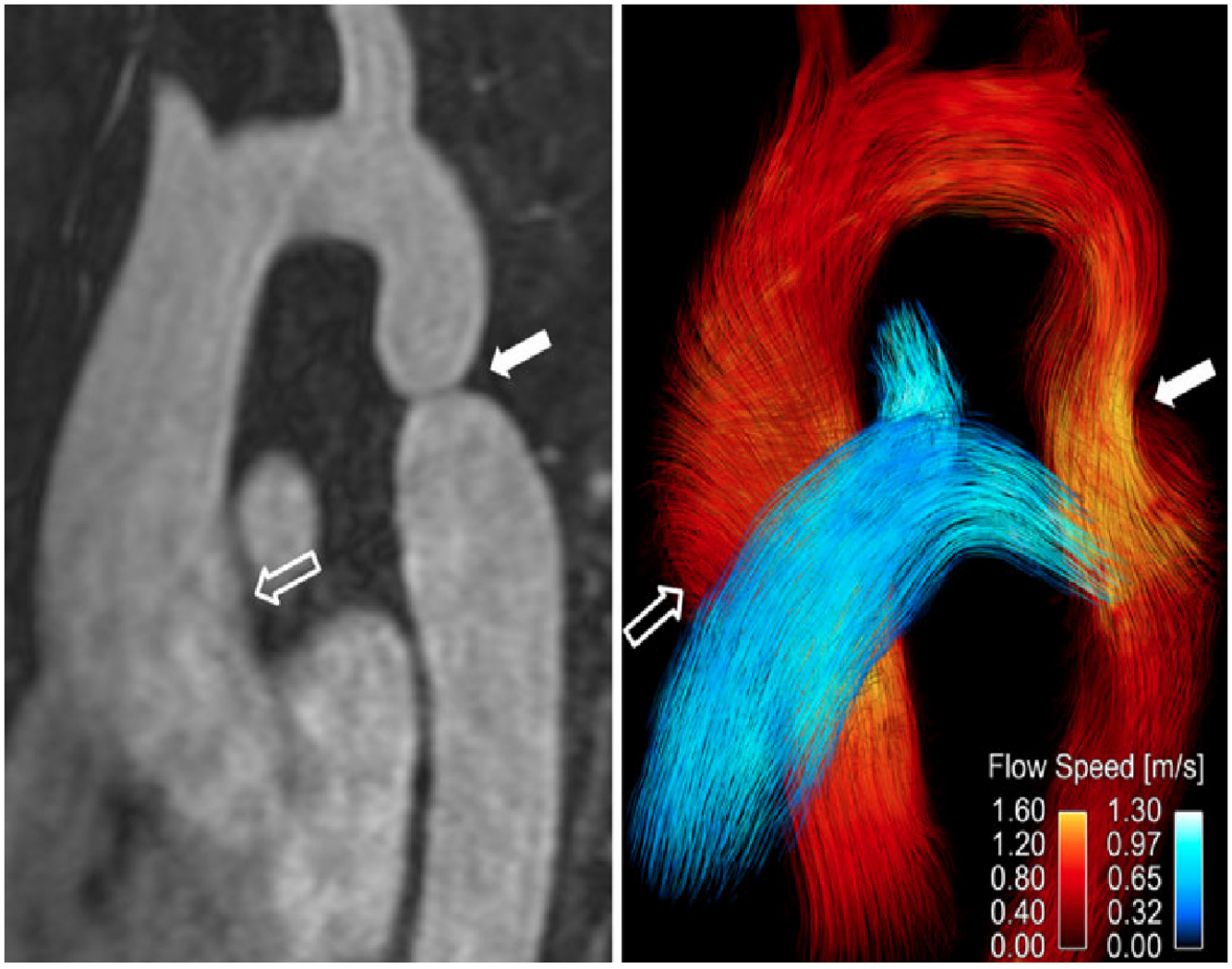

qualitative quantitative[1]

[1] figure borrowed from [Hope et al., 2013]

Example: diffusion imaging

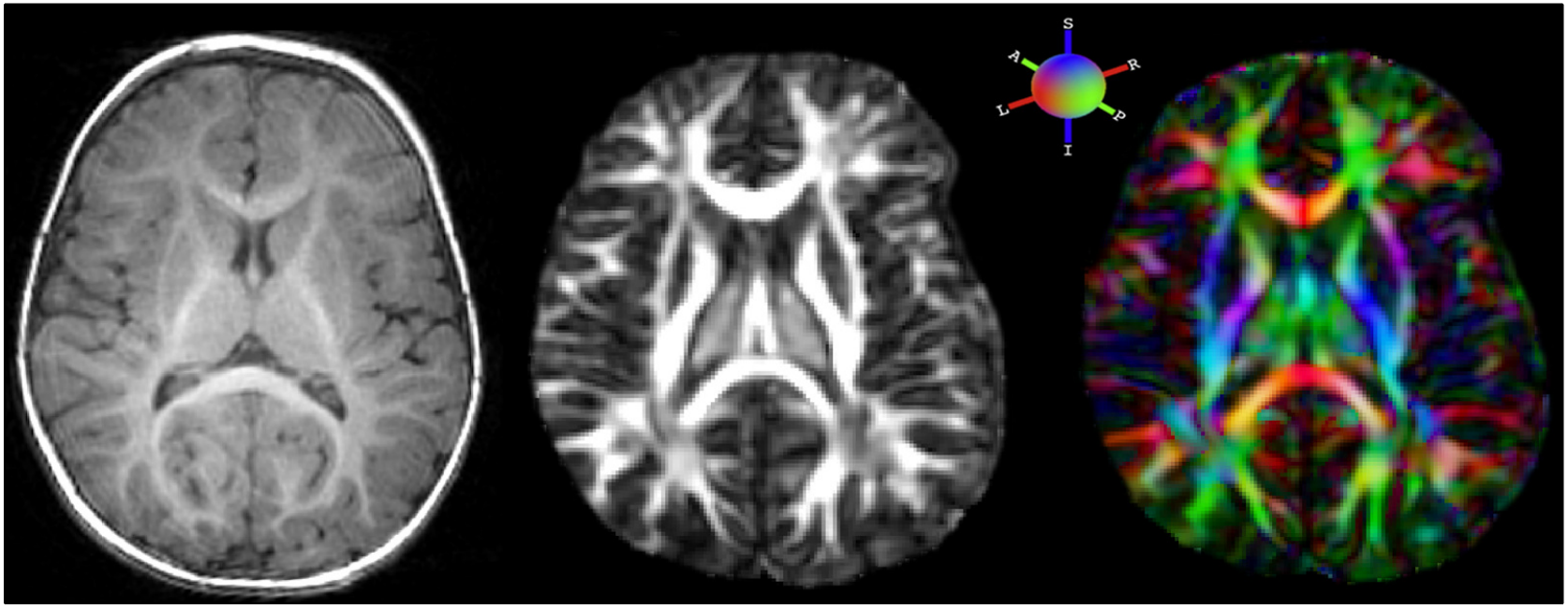

qualitative fractional anisotropy (FA) directional FA[2]

[2] figure borrowed from www.diffusion-imaging.com

Example: myelin water imaging

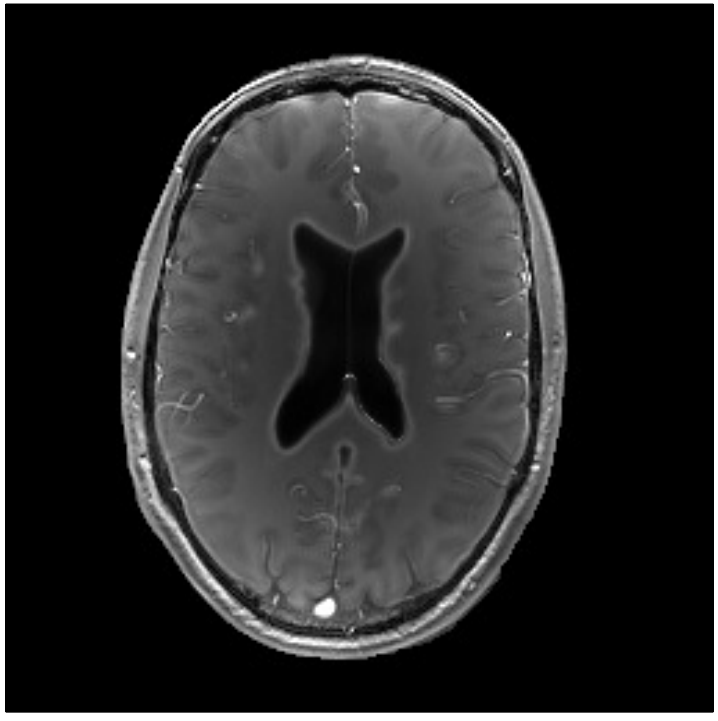

qualitative

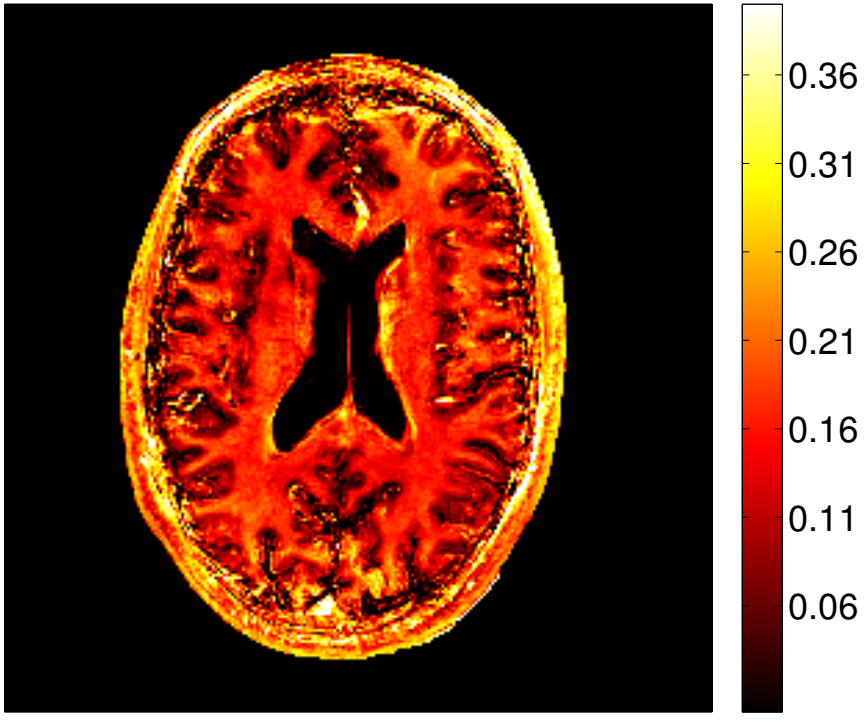

fast-relaxing fraction[3]

[3] figure adapted from [Nataraj et al., 2017a]

Quantitative MRI (QMRI)

Goal: rapidly and accurately localize biomarkers from MR data

Quantitative MRI (QMRI)

Goal: rapidly and accurately localize biomarkers from MR data

- biomarker measurable tissue property (*e.g.*, flow rate)
  that indicates a biological process (*e.g.*, blockage)
  characteristic to specific disorders (*e.g.*, stroke)

Quantitative MRI (QMRI)

Goal: rapidly and accurately localize biomarkers from MR data

- biomarker — measurable tissue property (*e.g.*, flow rate) that indicates a biological process (*e.g.*, blockage) characteristic to specific disorders (*e.g.*, stroke)
- localize — produce quantitative MR images

Quantitative MRI (QMRI)

Goal: rapidly and accurately localize biomarkers from MR data

- biomarker — measurable tissue property (*e.g.*, flow rate) that indicates a biological process (*e.g.*, blockage) characteristic to specific disorders (*e.g.*, stroke)
- localize — produce quantitative MR images
- accurately — physically realistic signal models
- rapidly — fast acquisition, fast estimation

Quantitative MRI (QMRI)

Goal: rapidly and accurately localize biomarkers from MR data

- biomarker — measurable tissue property (*e.g.*, flow rate) that indicates a biological process (*e.g.*, blockage) characteristic to specific disorders (*e.g.*, stroke)
- localize — produce quantitative MR images
- accurately — physically realistic signal models
- rapidly — fast acquisition, fast estimation

Challenge: rapidly vs. accurately often competing goals

- more accurate models typically depend on more markers
- precisely estimating more markers usually requires longer scans and more computation

Overview

Advances in Quantitative MRI:

- **Acquisition** [Ch. 4]
  How can we assemble fast, informative collections of scans to enable precise biomarker quantification?

Overview

Advances in Quantitative MRI:

- **Acquisition** [Ch. 4]
  How can we assemble fast, informative collections of scans to enable precise biomarker quantification?
- **Estimation** [Ch. 5]
  Given accurate models and informative data,
  how can we rapidly quantify these biomarkers?

Overview

Advances in Quantitative MRI:

- **Acquisition** [Ch. 4]
  How can we assemble fast, informative collections of scans to enable precise biomarker quantification?
- **Estimation** [Ch. 5]
  Given accurate models and informative data, how can we rapidly quantify these biomarkers?
- **Application** [Ch. 6]
  Using these tools, can we design a state-of-the-art biomarker?

Overview

Advances in Quantitative MRI:

- **Acquisition** [Ch. 4]
  How can we assemble fast, informative collections of scans to enable precise biomarker quantification?
- **Estimation** [Ch. 5]
  Given accurate models and informative data, how can we rapidly quantify these biomarkers?
- **Application** [Ch. 6]
  Using these tools, can we design a state-of-the-art biomarker?

Signal Model

After reconstruction, single voxel y_d in dth image modeled as

$$y_d = s_d(\mathbf{x}; \boldsymbol{\nu}, \mathbf{p}_d) + \epsilon_d \tag{1}$$

- $\mathbf{x} \in \mathbb{R}^L$ unknown parameters
- $\boldsymbol{\nu} \in \mathbb{R}^K$ "known" parameters
- $\mathbf{p}_d \in \mathbb{R}^A$ acquisition parameters
- $s_d : \mathbb{R}^{L+K+A} \mapsto \mathbb{C}$ dth signal model
- $\epsilon_d \in \mathbb{C}$ noise $\sim \mathbb{C}\mathcal{N}\left(0, \sigma_d^2\right)$

Signal Model

A *scan profile* is a set of D scans that produces at each voxel a measurement vector $\mathbf{y} := [y_1, \ldots, y_D]^\mathsf{T}$ modeled as

$$\mathbf{y} = \mathbf{s}(\mathbf{x}; \boldsymbol{\nu}, \mathbf{P}) + \boldsymbol{\epsilon} \tag{1}$$

- $\mathbf{x} \in \mathbb{R}^L$ unknown parameters
- $\boldsymbol{\nu} \in \mathbb{R}^K$ "known" parameters
- $\mathbf{P} := [\mathbf{p}_1, \ldots, \mathbf{p}_D]$ acquisition parameter matrix
- $\mathbf{s} : \mathbb{R}^{L+K+AD} \mapsto \mathbb{C}^D$ vector signal model
- $\boldsymbol{\epsilon} \sim \mathbb{C}\mathcal{N}(\mathbf{0}_D, \boldsymbol{\Sigma})$ noise, with $\boldsymbol{\Sigma} := \mathrm{diag}\left(\sigma_1^2, \ldots, \sigma_D^2\right)$

Signal Model

A *scan profile* is a set of D scans that produces at each voxel a measurement vector $\mathbf{y} := [y_1, \ldots, y_D]^\mathsf{T}$ modeled as

$$\mathbf{y} = \mathbf{s}(\mathbf{x}; \boldsymbol{\nu}, \mathbf{P}) + \boldsymbol{\epsilon} \tag{1}$$

- $\mathbf{x} \in \mathbb{R}^L$ unknown parameters
- $\boldsymbol{\nu} \in \mathbb{R}^K$ "known" parameters
- $\mathbf{P} := [\mathbf{p}_1, \ldots, \mathbf{p}_D]$ acquisition parameter matrix
- $\mathbf{s} : \mathbb{R}^{L+K+AD} \mapsto \mathbb{C}^D$ vector signal model
- $\boldsymbol{\epsilon} \sim \mathbb{C}\mathcal{N}(\mathbf{0}_D, \boldsymbol{\Sigma})$ noise, with $\boldsymbol{\Sigma} := \mathrm{diag}(\sigma_1^2, \ldots, \sigma_D^2)$

Task: design $\mathbf{P}$ to enable precise unbiased estimation of $\mathbf{x}$

Towards an Objective Function

When $\mathbf{s}$ is analytic in $\mathbf{x}$ (as is typical),

Fisher information characterizes unbiased estimator precision:

$$\mathbf{F}(\mathbf{x};\boldsymbol{\nu},\mathbf{P}) := (\nabla_{\mathbf{x}}\mathbf{s}(\mathbf{x};\boldsymbol{\nu},\mathbf{P}))^{\mathsf{H}}\boldsymbol{\Sigma}^{-1}\nabla_{\mathbf{x}}\mathbf{s}(\mathbf{x};\boldsymbol{\nu},\mathbf{P}). \tag{2}$$

Towards an Objective Function

When $\mathbf{s}$ is analytic in $\mathbf{x}$ (as is typical),
Fisher information characterizes unbiased estimator precision:

$$\mathbf{F}(\mathbf{x};\boldsymbol{\nu},\mathbf{P}) := (\nabla_{\mathbf{x}}\mathbf{s}(\mathbf{x};\boldsymbol{\nu},\mathbf{P}))^{\mathsf{H}}\boldsymbol{\Sigma}^{-1}\nabla_{\mathbf{x}}\mathbf{s}(\mathbf{x};\boldsymbol{\nu},\mathbf{P}). \tag{2}$$

When $\mathbf{F}$ is invertible, Cramér-Rao Bound (CRB) [Cramér, 1946] ensures covariance of unbiased estimates $\widehat{\mathbf{x}}$ of $\mathbf{x}$ satisfy

$$\operatorname{cov}\widehat{\mathbf{x}};\boldsymbol{\nu},\mathbf{P} \succeq \mathbf{F}^{-1}(\mathbf{x};\boldsymbol{\nu},\mathbf{P}). \tag{3}$$

Maximum-likelihood (ML) estimates achieve CRB asymptotically or (equivalently for Gaussian data) at sufficiently high SNR.

Towards an Objective Function

When $\mathbf{s}$ is analytic in $\mathbf{x}$ (as is typical),
Fisher information characterizes unbiased estimator precision:

$$\mathbf{F}(\mathbf{x}; \boldsymbol{\nu}, \mathbf{P}) := (\nabla_{\mathbf{x}} \mathbf{s}(\mathbf{x}; \boldsymbol{\nu}, \mathbf{P}))^{\mathsf{H}} \boldsymbol{\Sigma}^{-1} \nabla_{\mathbf{x}} \mathbf{s}(\mathbf{x}; \boldsymbol{\nu}, \mathbf{P}). \tag{2}$$

When $\mathbf{F}$ is invertible, Cramér-Rao Bound (CRB) [Cramér, 1946]
ensures covariance of unbiased estimates $\widehat{\mathbf{x}}$ of $\mathbf{x}$ satisfy

$$\operatorname{cov} \widehat{\mathbf{x}}; \boldsymbol{\nu}, \mathbf{P} \succeq \mathbf{F}^{-1}(\mathbf{x}; \boldsymbol{\nu}, \mathbf{P}). \tag{3}$$

Maximum-likelihood (ML) estimates achieve CRB asymptotically
or (equivalently for Gaussian data) at sufficiently high SNR.
Idea: choose $\mathbf{P}$ such that imprecision matrix $\mathbf{F}^{-1}$ "small"

Scan Design

Idea: choose $\mathbf{P}$ to minimize the objective

$$\Psi(\mathbf{x};\boldsymbol{\nu},\mathbf{P}) = \mathrm{tr}\Big(\mathbf{W}\mathbf{F}^{-1}(\mathbf{x};\boldsymbol{\nu},\mathbf{P})\mathbf{W}^{\mathsf{T}}\Big), \tag{4}$$

where $\mathbf{W} \in \mathbb{R}^{L\times L}$ is a pre-selected diagonal matrix of weights.

Scan Design

Idea: choose $\mathbf{P}$ to minimize the objective

$$\Psi(\mathbf{x};\boldsymbol{\nu},\mathbf{P}) = \mathrm{tr}\Big(\mathbf{W}\mathbf{F}^{-1}(\mathbf{x};\boldsymbol{\nu},\mathbf{P})\mathbf{W}^{\mathsf{T}}\Big), \tag{4}$$

where $\mathbf{W} \in \mathbb{R}^{L\times L}$ is a pre-selected diagonal matrix of weights.

Challenge: $\mathbf{x}, \boldsymbol{\nu}$ vary spatially

Scan Design

Idea: choose $\mathbf{P}$ to minimize the objective

$$\Psi(\mathbf{x};\boldsymbol{\nu},\mathbf{P}) = \mathrm{tr}\Big(\mathbf{W}\mathbf{F}^{-1}(\mathbf{x};\boldsymbol{\nu},\mathbf{P})\mathbf{W}^{\mathsf{T}}\Big), \tag{4}$$

where $\mathbf{W} \in \mathbb{R}^{L\times L}$ is a pre-selected diagonal matrix of weights.

Challenge: $\mathbf{x}, \boldsymbol{\nu}$ vary spatially

Two problems considered:

- min-max scan design [Nataraj et al., 2017b]

$$\check{\mathbf{P}} \in \left\{ \arg \min_{\mathbf{P}\in\mathbb{P}} \max_{\substack{\mathbf{x}\in\mathbb{X}^{\mathrm{t}} \\ \boldsymbol{\nu}\in\mathbb{N}^{\mathrm{t}}}} \Psi(\mathbf{x};\boldsymbol{\nu},\mathbf{P}) \right\} \tag{5}$$

  where $\mathbb{X}^{\mathrm{t}} \subseteq \mathbb{R}^{L}$ and $\mathbb{N}^{\mathrm{t}} \subseteq \mathbb{R}^{K}$ are "tight" ranges of interest and $\mathbb{P}$ is defined by acquisition/timing constraints

Scan Design

Idea: choose $\mathbf{P}$ to minimize the objective

$$\Psi(\mathbf{x};\boldsymbol{\nu},\mathbf{P}) = \mathrm{tr}\Big(\mathbf{W}\mathbf{F}^{-1}(\mathbf{x};\boldsymbol{\nu},\mathbf{P})\mathbf{W}^{\mathsf{T}}\Big), \tag{4}$$

where $\mathbf{W} \in \mathbb{R}^{L\times L}$ is a pre-selected diagonal matrix of weights.

Challenge: $\mathbf{x}, \boldsymbol{\nu}$ vary spatially

Two problems considered:

- min-max scan design [Nataraj et al., 2017b]

$$\check{\mathbf{P}} \in \left\{ \arg \min_{\mathbf{P}\in\mathbb{P}} \max_{\substack{\mathbf{x}\in\mathbb{X}^{\mathrm{t}} \\ \boldsymbol{\nu}\in\mathbb{N}^{\mathrm{t}}}} \Psi(\mathbf{x};\boldsymbol{\nu},\mathbf{P}) \right\} \tag{5}$$

- Bayesian scan design

$$\check{\mathbf{P}} \in \left\{ \arg \min_{\mathbf{P}\in\mathbb{P}} \mathrm{E}_{\mathbf{x},\boldsymbol{\nu}}(\Psi(\mathbf{x};\boldsymbol{\nu},\mathbf{P})) \right\} \tag{6}$$

Scan Design

Idea: choose $\mathbf{P}$ to minimize the objective

$$\Psi(\mathbf{x};\boldsymbol{\nu},\mathbf{P}) = \mathrm{tr}\Big(\mathbf{W}\mathbf{F}^{-1}(\mathbf{x};\boldsymbol{\nu},\mathbf{P})\mathbf{W}^{\mathsf{T}}\Big), \tag{4}$$

where $\mathbf{W} \in \mathbb{R}^{L\times L}$ is a pre-selected diagonal matrix of weights.

Challenge: $\mathbf{x}, \boldsymbol{\nu}$ vary spatially

Two problems considered:

- min-max scan design [Nataraj et al., 2017b]

$$\check{\mathbf{P}} \in \left\{ \arg \min_{\mathbf{P}\in\mathbb{P}} \max_{\substack{\mathbf{x}\in\mathbb{X}^{\mathrm{t}} \\ \boldsymbol{\nu}\in\mathbb{N}^{\mathrm{t}}}} \Psi(\mathbf{x};\boldsymbol{\nu},\mathbf{P}) \right\} \tag{5}$$

- Bayesian scan design

$$\check{\mathbf{P}} \in \left\{ \arg \min_{\mathbf{P}\in\mathbb{P}} \mathrm{E}_{\mathbf{x},\boldsymbol{\nu}}(\Psi(\mathbf{x};\boldsymbol{\nu},\mathbf{P})) \right\} \tag{6}$$

Detailed Example Study

Task: design fast acquisition for precise estimation of relaxation parameters T_1, T_2 in white/gray matter (WM/GM) of brain

Detailed Example Study

Task: design fast acquisition for precise estimation of relaxation parameters T_1, T_2 in white/gray matter (WM/GM) of brain

- Consider scan profiles consisting of two fast pulse sequences
  - Spoiled Gradient-Recalled Echo (SPGR) [Zur et al., 1991]
  - Dual-Echo Steady-State (DESS) [Redpath and Jones, 1988]

Detailed Example Study

Task: design fast acquisition for precise estimation of relaxation parameters T_1, T_2 in white/gray matter (WM/GM) of brain

- Consider scan profiles consisting of two fast pulse sequences
  - Spoiled Gradient-Recalled Echo (SPGR) [Zur et al., 1991]
  - Dual-Echo Steady-State (DESS) [Redpath and Jones, 1988]
- For each scan profile feasible under total time constraint:
  1. Let $\mathbf{s}$ model corresponding single-component signal
     - $\mathbf{x} \leftarrow [m_0, T_1, T_2]^{\mathsf{T}}$, where m_0 is a scale factor
     - $\boldsymbol{\nu} \leftarrow$ flip angle variation
     - $\mathbf{P} \leftarrow$ nominal flip angles, repetition times
  2. Optimize $\mathbf{P}$ subject to flip angle, sequence timing constraints
     - $\mathbf{W} \leftarrow \mathrm{diag}(0, 0.1, 1)$ emphasizes T_1, T_2 est roughly equally
     - $\mathbb{X}^{\mathrm{t}}$ chosen to focus on WM/GM at 3T field strength
     - $\mathbb{N}^{\mathrm{t}}$ chosen to allow 10% flip angle variation

Scan Profile Comparison

(#SPGR, #DESS) Profiles	$(2,1)$	$(1,1)$	$(0,2)$
SPGR nom. flip (deg)	(15, 5)	15	–
DESS nom. flip (deg)	30	10	(35, 10)
SPGR rep. times (ms)	(12.2, 12.2)	13.9	–
DESS rep. times (ms)	17.5	28.0	(24.4, 17.5)
optimal max cost	4.0	4.9	**3.5**

Scan Profile Comparison

(#SPGR, #DESS) Profiles	(2, 1)	(1, 1)	(0, 2)
SPGR nom. flip (deg)	(15, 5)	15	–
DESS nom. flip (deg)	30	10	(35, 10)
SPGR rep. times (ms)	(12.2, 12.2)	13.9	–
DESS rep. times (ms)	17.5	28.0	(24.4, 17.5)
optimal max cost	4.0	4.9	**3.5**

Main finding: 2 DESS sequences can yield T_1, T_2 WM/GM estimates that are at least as precise as T_1, T_2 estimates from SPGR/DESS scan profiles, under this competitive time constraint.

Experimental Setup

Candidate $(2,1)$, $(1,1)$, $(0,2)$ SPGR/DESS scan profiles

- Prescribed optimized nominal flip angles, repetition times
- Used $256 \times 256 \times 8$ 3D matrix over $24 \times 24 \times 4$cm FOV
- Required **1m37s** scan time for each profile

Experimental Setup

Candidate $(2,1)$, $(1,1)$, $(0,2)$ SPGR/DESS scan profiles

- Prescribed optimized nominal flip angles, repetition times
- Used $256 \times 256 \times 8$ 3D matrix over $24 \times 24 \times 4$cm FOV
- Required **1m37s** scan time for each profile

Reference scan profile

- Four inversion recovery (IR) scans for T_1 estimation
- Four spin-echo (SE) scans for T_2 estimation
- 256×256 matrix over $24 \times 24 \times 0.5$cm FOV
- Required **40m58s** scan time total

Experimental Setup

Candidate $(2,1)$, $(1,1)$, $(0,2)$ SPGR/DESS scan profiles

- Prescribed optimized nominal flip angles, repetition times
- Used $256 \times 256 \times 8$ 3D matrix over $24 \times 24 \times 4$cm FOV
- Required **1m37s** scan time for each profile

Reference scan profile

- Four inversion recovery (IR) scans for T_1 estimation
- Four spin-echo (SE) scans for T_2 estimation
- 256×256 matrix over $24 \times 24 \times 0.5$cm FOV
- Required **40m58s** scan time total

Bloch-Siegert (BS) acquisition for separate flip angle calibration

- Acquired 2 BS-shifted 3D SPGR scans in 1m40s total
- Used for T_1, T_2 est from both candidate and reference profiles

Phantom Accuracy Results

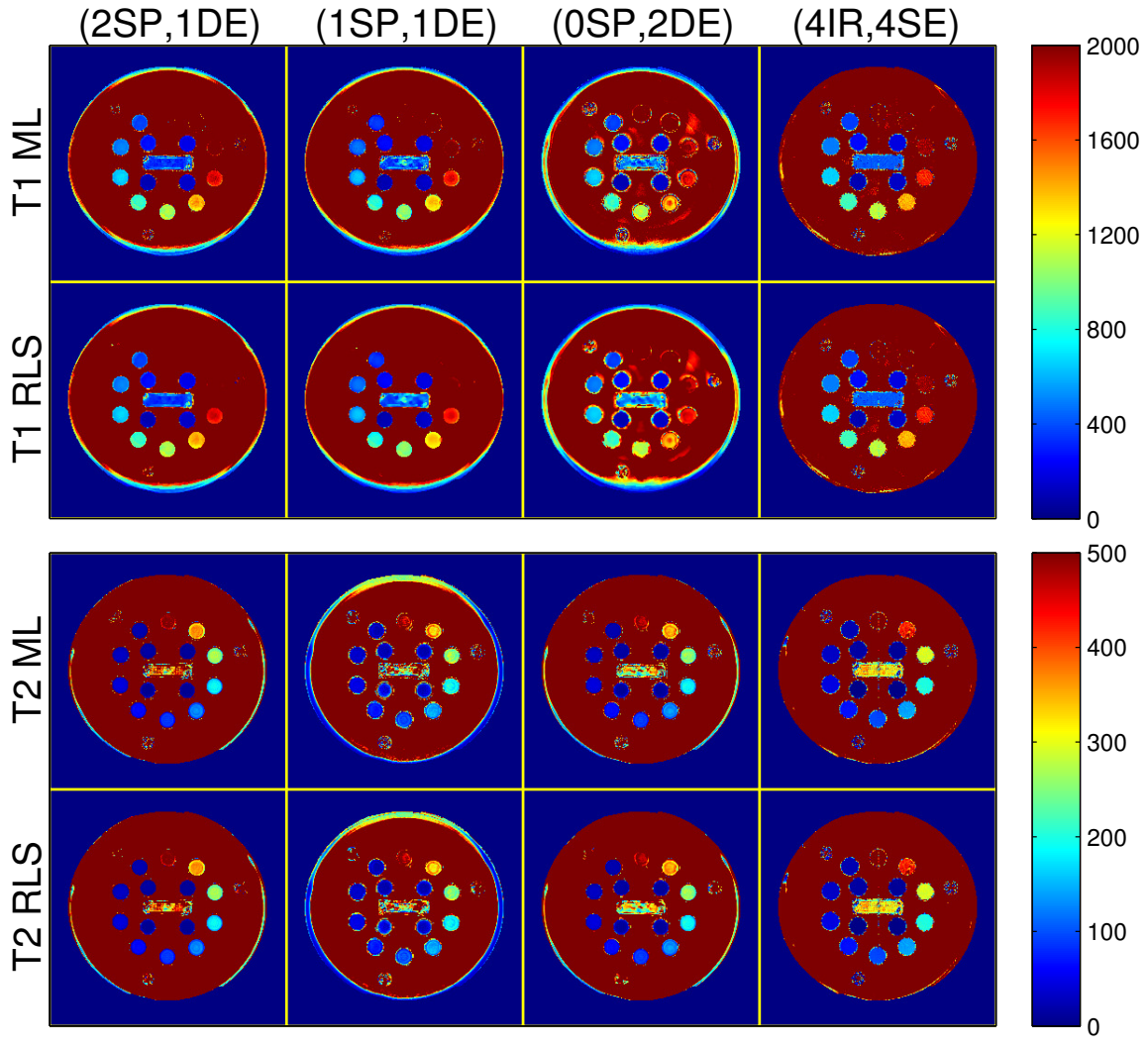

Figure 1: Colorbar ranges in ms.

Phantom Accuracy Results

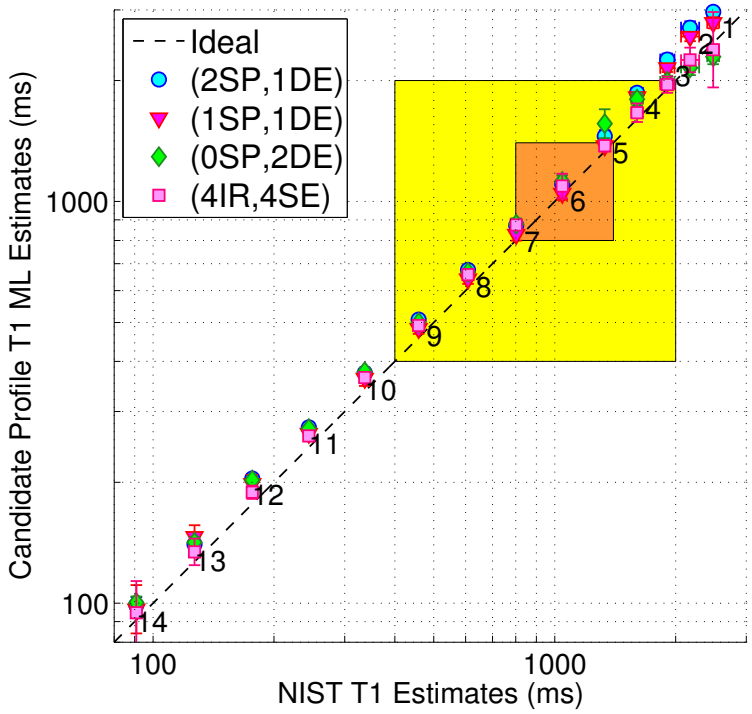

(a) $\widehat{T}_1^{\mathrm{ML}}$ Estimates

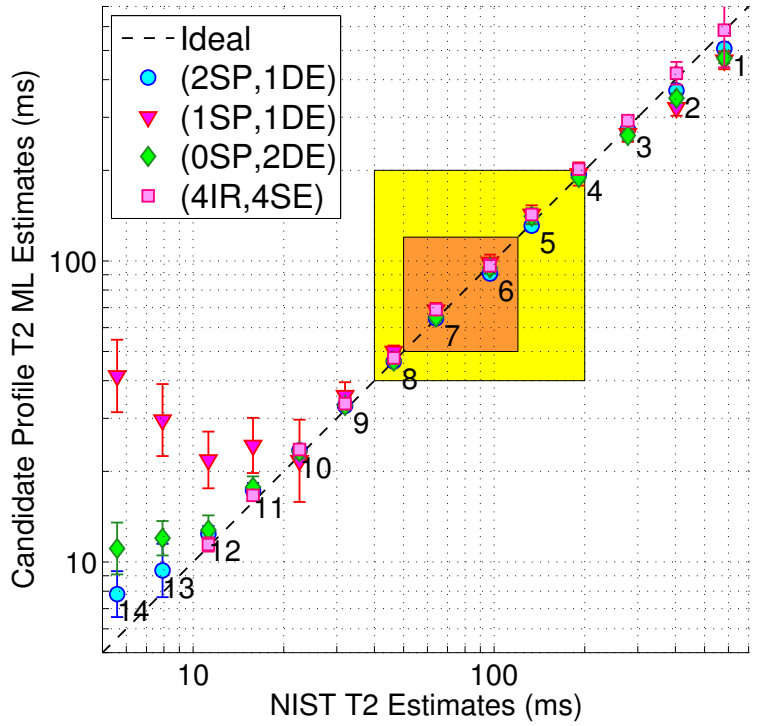

(b) $\widehat{T}_2^{\mathrm{ML}}$ Estimates

Compared against NIST NMR measurements [Keenan et al., 2016]

Phantom Precision Results

- Repeated each profile 10 times
- Estimated T_1, T_2 std dev of typical voxel across repetitions

Phantom Precision Results

	(2, 1)	(1, 1)	(0, 2)
V5 $\widehat{\sigma}_{\widehat{T}_1^{\mathrm{ML}}}$	50 ± 12	$40 \pm 10.$	39 ± 9.4
V6 $\widehat{\sigma}_{\widehat{T}_1^{\mathrm{ML}}}$	70 ± 18	60 ± 15	60 ± 16
V7 $\widehat{\sigma}_{\widehat{T}_1^{\mathrm{ML}}}$	60 ± 13	50 ± 13	50 ± 13
V5 $\widehat{\sigma}_{\widehat{T}_2^{\mathrm{ML}}}$	2.6 ± 0.63	6 ± 1.4	3.5 ± 0.84
V6 $\widehat{\sigma}_{\widehat{T}_2^{\mathrm{ML}}}$	1.9 ± 0.46	5 ± 1.1	2.3 ± 0.54
V7 $\widehat{\sigma}_{\widehat{T}_2^{\mathrm{ML}}}$	1.4 ± 0.34	3.4 ± 0.80	1.5 ± 0.35
$\sqrt{\text{opt max cost}}$ estimate	8.9 ± 1.8	11 ± 2.6	$\mathbf{8.3 \pm 2.1}$

Table 1: Pooled sample standard deviations $\pm$ pooled standard errors of sample standard deviations (ms), from optimized SPGR/DESS profiles.

Phantom Precision Results

	(2, 1)	(1, 1)	(0, 2)
V5 $\widehat{\sigma}_{\widehat{T}_1^{\mathrm{ML}}}$	50 ± 12	$40 \pm 10.$	39 ± 9.4
V6 $\widehat{\sigma}_{\widehat{T}_1^{\mathrm{ML}}}$	70 ± 18	60 ± 15	60 ± 16
V7 $\widehat{\sigma}_{\widehat{T}_1^{\mathrm{ML}}}$	60 ± 13	50 ± 13	50 ± 13
V5 $\widehat{\sigma}_{\widehat{T}_2^{\mathrm{ML}}}$	2.6 ± 0.63	6 ± 1.4	3.5 ± 0.84
V6 $\widehat{\sigma}_{\widehat{T}_2^{\mathrm{ML}}}$	1.9 ± 0.46	5 ± 1.1	2.3 ± 0.54
V7 $\widehat{\sigma}_{\widehat{T}_2^{\mathrm{ML}}}$	1.4 ± 0.34	3.4 ± 0.80	1.5 ± 0.35
$\sqrt{\text{opt max cost}}$ estimate	8.9 ± 1.8	11 ± 2.6	$\mathbf{8.3 \pm 2.1}$

Table 1: Pooled sample standard deviations $\pm$ pooled standard errors of sample standard deviations (ms), from optimized SPGR/DESS profiles.

Similar trends across profiles of empirical vs. theoretical std dev!

Summary

Contributions

- MR scan design method for precise parameter estimation
- Fast SPGR/DESS scan profile for T_1, T_2 estimation in brain

Summary

Contributions

- MR scan design method for precise parameter estimation
- Fast SPGR/DESS scan profile for T_1, T_2 estimation in brain
    - Phantom (and omitted simulation) results validate method as a predictor of unbiased estimation precision.

Summary

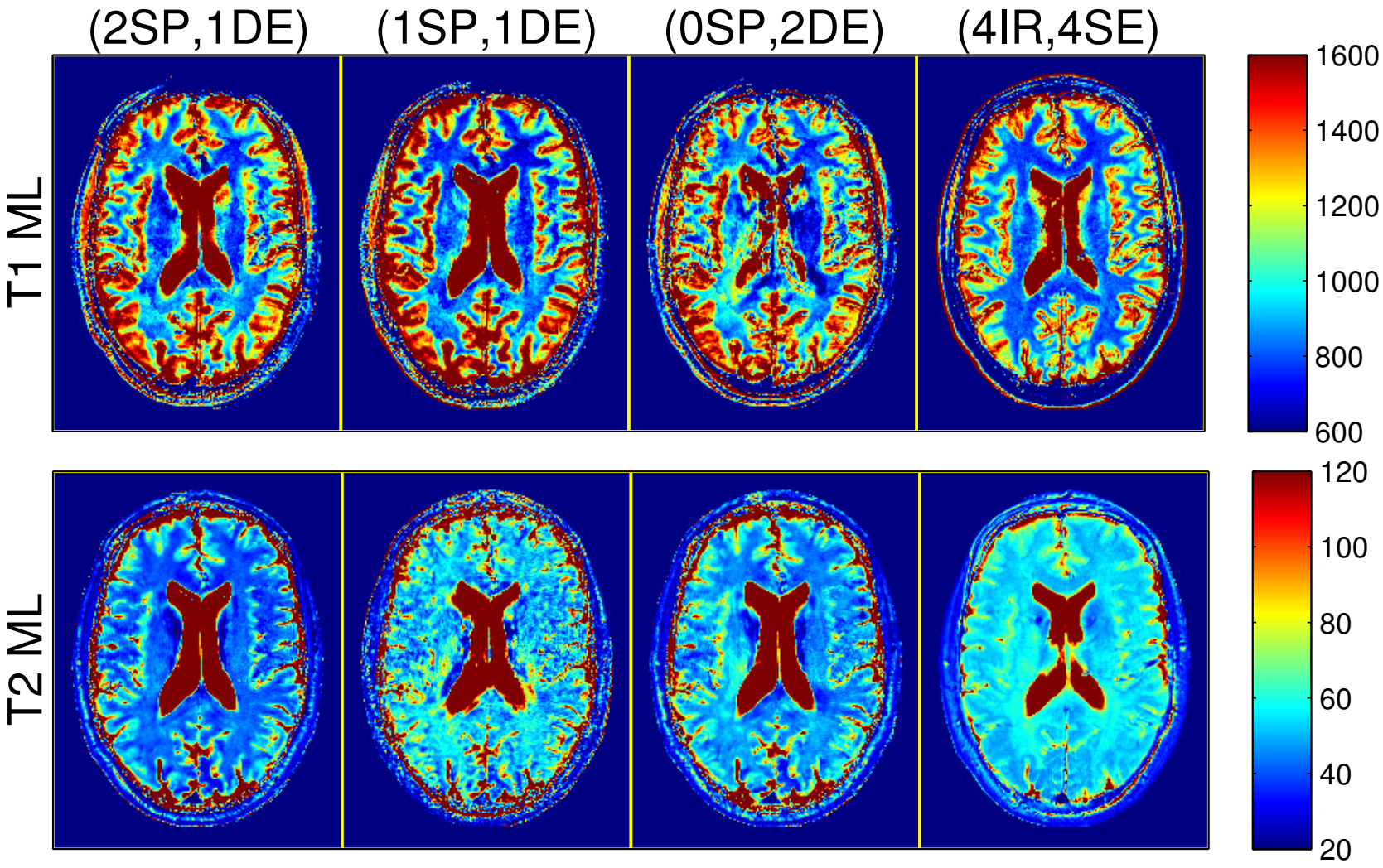

Figure 2: Colorbar ranges in ms.

Summary

Contributions

- MR scan design method for precise parameter estimation
- Fast SPGR/DESS scan profile for T_1, T_2 estimation in brain
  - Phantom (and omitted simulation) results validate method as a predictor of unbiased estimation precision.
  - *In vivo* results reveal discrepancies (especially in T_2 estimates), suggesting T_1, T_2 estimates sensitive to model mismatch.

Summary

Contributions

- MR scan design method for precise parameter estimation
- Fast SPGR/DESS scan profile for T_1, T_2 estimation in brain
  - Phantom (and omitted simulation) results validate method as a predictor of unbiased estimation precision.
  - *In vivo* results reveal discrepancies (especially in T_2 estimates), suggesting T_1, T_2 estimates sensitive to model mismatch.

How to address in vivo model mismatch?

- More accurate *in vivo* signal models
- More scalable parameter estimation

Overview

Advances in Quantitative MRI:

- **Acquisition** [Ch. 4]
  How can we assemble fast, informative collections of scans to enable precise biomarker quantification?
- **Estimation** [Ch. 5]
  Given accurate models and informative data, how can we rapidly quantify these biomarkers?
- **Application** [Ch. 6]
  Using these tools, can we design a state-of-the-art biomarker?

Signal Model

Given: at every voxel, measurement vector $\mathbf{y} \in \mathbb{C}^D$ modeled as

$$\mathbf{y} = \mathbf{s}(\mathbf{x}, \boldsymbol{\nu}) + \boldsymbol{\epsilon} \tag{7}$$

- $\mathbf{x} \in \mathbb{R}^L$ unknown parameters
- $\boldsymbol{\nu} \in \mathbb{R}^K$ "known" parameters
- $\mathbf{s} : \mathbb{R}^{L+K} \mapsto \mathbb{C}^D$ vector signal model
- $\boldsymbol{\epsilon} \in \mathbb{C}^D$ noise $\sim \mathbb{C}\mathcal{N}(\mathbf{0}_D, \boldsymbol{\Sigma})$

Signal Model

Given: at every voxel, measurement vector $\mathbf{y} \in \mathbb{C}^D$ modeled as

$$\mathbf{y} = \mathbf{s}(\mathbf{x}, \boldsymbol{\nu}) + \boldsymbol{\epsilon} \tag{7}$$

- $\mathbf{x} \in \mathbb{R}^L$ unknown parameters
- $\boldsymbol{\nu} \in \mathbb{R}^K$ "known" parameters
- $\mathbf{s} : \mathbb{R}^{L+K} \mapsto \mathbb{C}^D$ vector signal model
- $\boldsymbol{\epsilon} \in \mathbb{C}^D$ noise $\sim \mathbb{C}\mathcal{N}(\mathbf{0}_D, \boldsymbol{\Sigma})$

Task: design fast voxel-by-voxel estimator $\widehat{\mathbf{x}}(\mathbf{y}, \boldsymbol{\nu})$

Prior Work

Task: design fast voxel-by-voxel estimator $\widehat{\mathbf{x}}(\mathbf{y}, \boldsymbol{\nu})$

Challenges:

- signal $\mathbf{s}$ often nonlinear in $\mathbf{x}$: non-convex inverse problems
- signal $\mathbf{s}$ might be difficult to write in closed form

Prior Work

Task: design fast voxel-by-voxel estimator $\widehat{\mathbf{x}}(\mathbf{y}, \boldsymbol{\nu})$

Challenges:

- signal $\mathbf{s}$ often nonlinear in $\mathbf{x}$: non-convex inverse problems
- signal $\mathbf{s}$ might be difficult to write in closed form

Conventional Approaches:

- gradient-based local optimization
  - initialization-dependent solution
  - requires signal gradients

Prior Work

Task: design fast voxel-by-voxel estimator $\widehat{\mathbf{x}}(\mathbf{y}, \boldsymbol{\nu})$

Challenges:

- signal $\mathbf{s}$ often nonlinear in $\mathbf{x}$: non-convex inverse problems
- signal $\mathbf{s}$ might be difficult to write in closed form

Conventional Approaches:

- gradient-based local optimization
  - initialization-dependent solution
  - requires signal gradients
- stochastic methods (*e.g.*, simulated annealing)
  - unclear convergence analysis [Bertsimas and Tsitsiklis, 1993]
  - several unintuitive tuning parameters

Prior Work

Task: design fast voxel-by-voxel estimator $\widehat{\mathbf{x}}(\mathbf{y}, \boldsymbol{\nu})$

Challenges:

- signal $\mathbf{s}$ often nonlinear in $\mathbf{x}$: non-convex inverse problems
- signal $\mathbf{s}$ might be difficult to write in closed form

Conventional Approaches:

- gradient-based local optimization
  - initialization-dependent solution
  - requires signal gradients
- stochastic methods (*e.g.*, simulated annealing)
  - unclear convergence analysis [Bertsimas and Tsitsiklis, 1993]
  - several unintuitive tuning parameters
- dictionary-based grid search

Motivation

Grid search computational costs

	L	$\sim$number dictionary atoms
1-compartment relaxivity	3	$\sim 100^2$

Motivation

Grid search computational costs

	L	$\sim$number dictionary atoms
1-compartment relaxivity	3	$\sim 100^2$
flow velocity	4	$\sim 100^3$
diffusivity tensor	7	$\sim 100^6$
2-3 compartment relaxivity	6-10	$\sim 100^5 - 100^9$

Motivation

Grid search computational costs

	L	$\sim$number dictionary atoms
1-compartment relaxivity	3	$\sim 100^2$
flow velocity	4	$\sim 100^3$
diffusivity tensor	7	$\sim 100^6$
2-3 compartment relaxivity	6-10	$\sim 100^5 - 100^9$

Can we scale computation with L more gracefully?

Machine Learning for QMRI Parameter Estimation

Idea: learn a *nonlinear* estimator from simulated training data

Machine Learning for QMRI Parameter Estimation

Idea: learn a *nonlinear* estimator from simulated training data

- sample $(\mathbf{x}_1, \boldsymbol{\nu}_1, \boldsymbol{\epsilon}_1), \ldots, (\mathbf{x}_N, \boldsymbol{\nu}_N, \boldsymbol{\epsilon}_N)$ from prior distributions
- simulate image data vectors $\mathbf{y}_1, \ldots, \mathbf{y}_N$ via signal model $\mathbf{s}$

Machine Learning for QMRI Parameter Estimation

Idea: learn a *nonlinear* estimator from simulated training data

- sample $(\mathbf{x}_1, \boldsymbol{\nu}_1, \boldsymbol{\epsilon}_1), \ldots, (\mathbf{x}_N, \boldsymbol{\nu}_N, \boldsymbol{\epsilon}_N)$ from prior distributions
- simulate image data vectors $\mathbf{y}_1, \ldots, \mathbf{y}_N$ via signal model $\mathbf{s}$
- design *nonlinear* functions $\widehat{x}_l(\cdot) := \widehat{h}_l(\cdot) + \widehat{b}_l$ for $l \in \{1, \ldots, L\}$ that map each $\mathbf{q}_n := [\mathrm{Re}(\mathbf{y}_n)^\mathsf{T}, \mathrm{Im}(\mathbf{y}_n)^\mathsf{T}, \boldsymbol{\nu}_n^\mathsf{T}]^\mathsf{T} \in \mathcal{Q}$ to $x_{l,n} \in \mathbb{R}$

Machine Learning for QMRI Parameter Estimation

Idea: learn a *nonlinear* estimator from simulated training data

- sample $(\mathbf{x}_1, \boldsymbol{\nu}_1, \epsilon_1), \ldots, (\mathbf{x}_N, \boldsymbol{\nu}_N, \epsilon_N)$ from prior distributions
- simulate image data vectors $\mathbf{y}_1, \ldots, \mathbf{y}_N$ via signal model $\mathbf{s}$
- design *nonlinear* functions $\widehat{x}_l(\cdot) := \widehat{h}_l(\cdot) + \widehat{b}_l$ for $l \in \{1, \ldots, L\}$ that map each $\mathbf{q}_n := [\mathrm{Re}(\mathbf{y}_n)^{\mathsf{T}}, \mathrm{Im}(\mathbf{y}_n)^{\mathsf{T}}, \boldsymbol{\nu}_n^{\mathsf{T}}]^{\mathsf{T}} \in \mathcal{Q}$ to $x_{l,n} \in \mathbb{R}$

$$\left(\widehat{h}_l, \widehat{b}_l\right) \in \left\{ \arg \min_{\substack{h_l \\ b_l \in \mathbb{R}}} \frac{1}{N} \sum_{n=1}^{N} \left(h_l(\mathbf{q}_n) + b_l - x_{l,n}\right)^2 \right\}$$

Machine Learning for QMRI Parameter Estimation

Idea: learn a *nonlinear* estimator from simulated training data

- sample $(\mathbf{x}_1, \boldsymbol{\nu}_1, \epsilon_1), \ldots, (\mathbf{x}_N, \boldsymbol{\nu}_N, \epsilon_N)$ from prior distributions
- simulate image data vectors $\mathbf{y}_1, \ldots, \mathbf{y}_N$ via signal model $\mathbf{s}$
- design *nonlinear* functions $\widehat{x}_l(\cdot) := \widehat{h}_l(\cdot) + \widehat{b}_l$ for $l \in \{1, \ldots, L\}$ that map each $\mathbf{q}_n := [\mathrm{Re}(\mathbf{y}_n)^\mathsf{T}, \mathrm{Im}(\mathbf{y}_n)^\mathsf{T}, \boldsymbol{\nu}_n^\mathsf{T}]^\mathsf{T} \in \mathcal{Q}$ to $x_{l,n} \in \mathbb{R}$

$$\left(\widehat{h}_l, \widehat{b}_l\right) \in \left\{ \arg \min_{\substack{h_l \\ b_l \in \mathbb{R}}} \frac{1}{N} \sum_{n=1}^{N} \left(h_l(\mathbf{q}_n) + b_l - x_{l,n}\right)^2 \right\} \quad \text{ill-posed!}$$

Machine Learning for QMRI Parameter Estimation

Idea: learn a *nonlinear* estimator from simulated training data

- sample $(\mathbf{x}_1, \boldsymbol{\nu}_1, \epsilon_1), \ldots, (\mathbf{x}_N, \boldsymbol{\nu}_N, \epsilon_N)$ from prior distributions
- simulate image data vectors $\mathbf{y}_1, \ldots, \mathbf{y}_N$ via signal model $\mathbf{s}$
- design *nonlinear* functions $\widehat{x}_l(\cdot) := \widehat{h}_l(\cdot) + \widehat{b}_l$ for $l \in \{1, \ldots, L\}$ that map each $\mathbf{q}_n := [\mathrm{Re}(\mathbf{y}_n)^\mathsf{T}, \mathrm{Im}(\mathbf{y}_n)^\mathsf{T}, \boldsymbol{\nu}_n^\mathsf{T}]^\mathsf{T} \in \mathcal{Q}$ to $x_{l,n} \in \mathbb{R}$

$$\left(\widehat{h}_l, \widehat{b}_l\right) \in \left\{ \arg \min_{\substack{h_l \in \mathbb{H} \\ b_l \in \mathbb{R}}} \frac{1}{N} \sum_{n=1}^{N} (h_l(\mathbf{q}_n) + b_l - x_{l,n})^2 + \rho_l \|h_l\|_{\mathbb{H}}^2 \right\} \quad (8)$$

Solution: Param Estimation via Regression with Kernels (PERK)

[Nataraj et al., 2018]

- restrict optimization to a certain rich function space $\mathbb{H}$
- optimal $\widehat{h}_l \in \mathbb{H}$ takes form $\widehat{h}_l = \sum_{n=1}^{N} \widehat{a}_{l,n} k(\cdot, \mathbf{q}_n)$

[Schölkopf et al., 2001]

PERK in a 1-D Toy Problem

Task: estimate T_2, given samples from $y = \exp(-T_E/T_2) + \epsilon$

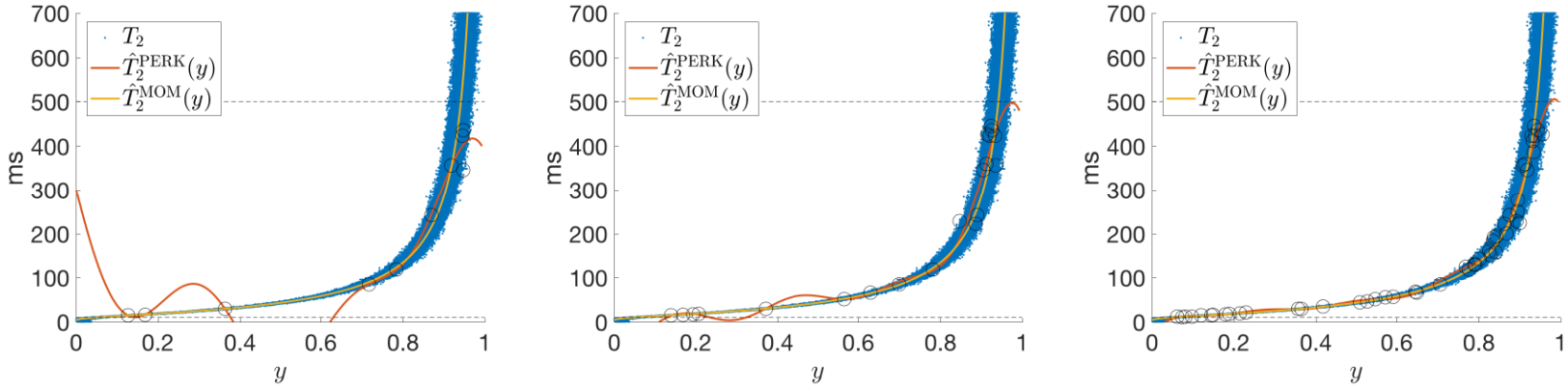

(a) $N \leftarrow 10$ **(b)** $N \leftarrow 20$ **(c)** $N \leftarrow 50$

Compare: $\widehat{T}_2^{\mathrm{PERK}}$ with method-of-moments (MOM) estimator

$$\widehat{T}_2^{\mathrm{MOM}}(\cdot) := -T_E/\log|\cdot|$$

(PERK more useful when good MOM estimator unavailable)

PERK Solution

Non-iterative closed-form solution, for $l \in \{1, \ldots, L\}$:

$$\widehat{x}_l(\cdot) = \mathbf{x}_l^{\mathsf{T}} \left(\frac{1}{N} \mathbf{1}_N + \mathbf{M}(\mathbf{K}\mathbf{M} + N\rho_l \mathbf{I}_N)^{-1} \left(\mathbf{k}(\cdot) - \frac{1}{N} \mathbf{K}\mathbf{1}_N \right) \right) \quad (9)$$

- $\mathbf{x}_l := [x_{l,1}, \ldots, x_{l,N}]^{\mathsf{T}}$ training pt regressands

PERK Solution

Non-iterative closed-form solution, for $l \in \{1, \ldots, L\}$:

$$\widehat{x}_l(\cdot) = \mathbf{x}_l^{\mathsf{T}} \left(\frac{1}{N} \mathbf{1}_N + \mathbf{M}(\mathbf{K}\mathbf{M} + N\rho_l \mathbf{I}_N)^{-1} \left(\mathbf{k}(\cdot) - \frac{1}{N} \mathbf{K}\mathbf{1}_N \right) \right) \quad (9)$$

- $\mathbf{x}_l := [x_{l,1}, \ldots, x_{l,N}]^{\mathsf{T}}$ training pt regressands
- $\mathbf{K} := \begin{bmatrix} k(\mathbf{q}_1, \mathbf{q}_1) & \cdots & k(\mathbf{q}_1, \mathbf{q}_N) \\ \vdots & \ddots & \vdots \\ k(\mathbf{q}_N, \mathbf{q}_1) & \cdots & k(\mathbf{q}_N, \mathbf{q}_N) \end{bmatrix}$ Gram matrix

PERK Solution

Non-iterative closed-form solution, for $l \in \{1, \ldots, L\}$:

$$\widehat{x}_l(\cdot) = \mathbf{x}_l^{\mathsf{T}} \left(\frac{1}{N} \mathbf{1}_N + \mathbf{M}(\mathbf{K}\mathbf{M} + N\rho_l \mathbf{I}_N)^{-1} \left(\mathbf{k}(\cdot) - \frac{1}{N} \mathbf{K}\mathbf{1}_N \right) \right) \quad (9)$$

- $\mathbf{x}_l := [x_{l,1}, \ldots, x_{l,N}]^{\mathsf{T}}$ — training pt regressands
- $\mathbf{K} := \begin{bmatrix} k(\mathbf{q}_1, \mathbf{q}_1) & \cdots & k(\mathbf{q}_1, \mathbf{q}_N) \\ \vdots & \ddots & \vdots \\ k(\mathbf{q}_N, \mathbf{q}_1) & \cdots & k(\mathbf{q}_N, \mathbf{q}_N) \end{bmatrix}$ — Gram matrix
- $\mathbf{M} := \mathbf{I}_N - \frac{1}{N} \mathbf{1}_N \mathbf{1}_N^{\mathsf{T}}$ — de-meaning operator

PERK Solution

Non-iterative closed-form solution, for $l \in \{1, \ldots, L\}$:

$$\widehat{x}_l(\cdot) = \mathbf{x}_l^{\mathsf{T}} \left(\frac{1}{N} \mathbf{1}_N + \mathbf{M}(\mathbf{K}\mathbf{M} + N\rho_l \mathbf{I}_N)^{-1} \left(\mathbf{k}(\cdot) - \frac{1}{N} \mathbf{K}\mathbf{1}_N \right) \right) \quad (9)$$

- $\mathbf{x}_l := [x_{l,1}, \ldots, x_{l,N}]^{\mathsf{T}}$ — training pt regressands
- $\mathbf{K} := \begin{bmatrix} k(\mathbf{q}_1, \mathbf{q}_1) & \cdots & k(\mathbf{q}_1, \mathbf{q}_N) \\ \vdots & \ddots & \vdots \\ k(\mathbf{q}_N, \mathbf{q}_1) & \cdots & k(\mathbf{q}_N, \mathbf{q}_N) \end{bmatrix}$ — Gram matrix
- $\mathbf{M} := \mathbf{I}_N - \frac{1}{N} \mathbf{1}_N \mathbf{1}_N^{\mathsf{T}}$ — de-meaning operator
- $\mathbf{k}(\cdot) := [k(\cdot, \mathbf{q}_1), \ldots, k(\cdot, \mathbf{q}_N)]^{\mathsf{T}}$ — nonlin kernel embedding

PERK Solution

Non-iterative closed-form solution, for $l \in \{1, \ldots, L\}$:

$$\widehat{x}_l(\cdot) = \mathbf{x}_l^{\mathsf{T}} \left(\frac{1}{N} \mathbf{1}_N + \mathbf{M}(\mathbf{K}\mathbf{M} + N\rho_l \mathbf{I}_N)^{-1} \left(\mathbf{k}(\cdot) - \frac{1}{N} \mathbf{K} \mathbf{1}_N \right) \right) \quad (9)$$

- $\mathbf{x}_l := [x_{l,1}, \ldots, x_{l,N}]^{\mathsf{T}}$ — training pt regressands
- $\mathbf{K} := \begin{bmatrix} k(\mathbf{q}_1, \mathbf{q}_1) & \cdots & k(\mathbf{q}_1, \mathbf{q}_N) \\ \vdots & \ddots & \vdots \\ k(\mathbf{q}_N, \mathbf{q}_1) & \cdots & k(\mathbf{q}_N, \mathbf{q}_N) \end{bmatrix}$ — Gram matrix
- $\mathbf{M} := \mathbf{I}_N - \frac{1}{N} \mathbf{1}_N \mathbf{1}_N^{\mathsf{T}}$ — de-meaning operator
- $\mathbf{k}(\cdot) := [k(\cdot, \mathbf{q}_1), \ldots, k(\cdot, \mathbf{q}_N)]^{\mathsf{T}}$ — nonlin kernel embedding

Can we scale computation with L more gracefully?

- Perhaps, since (9) separable in $l \in \{1, \ldots, L\}$ by construction

PERK Solution

Non-iterative closed-form solution, for $l \in \{1, \ldots, L\}$:

$$\widehat{x}_l(\cdot) = \mathbf{x}_l^{\mathsf{T}} \left(\frac{1}{N} \mathbf{1}_N + \mathbf{M}(\mathbf{K}\mathbf{M} + N\rho_l \mathbf{I}_N)^{-1} \left(\mathbf{k}(\cdot) - \frac{1}{N} \mathbf{K} \mathbf{1}_N \right) \right) \quad (9)$$

- $\mathbf{x}_l := [x_{l,1}, \ldots, x_{l,N}]^{\mathsf{T}}$ — training pt regressands
- $\mathbf{K} := \begin{bmatrix} k(\mathbf{q}_1, \mathbf{q}_1) & \cdots & k(\mathbf{q}_1, \mathbf{q}_N) \\ \vdots & \ddots & \vdots \\ k(\mathbf{q}_N, \mathbf{q}_1) & \cdots & k(\mathbf{q}_N, \mathbf{q}_N) \end{bmatrix}$ — Gram matrix
- $\mathbf{M} := \mathbf{I}_N - \frac{1}{N} \mathbf{1}_N \mathbf{1}_N^{\mathsf{T}}$ — de-meaning operator
- $\mathbf{k}(\cdot) := [k(\cdot, \mathbf{q}_1), \ldots, k(\cdot, \mathbf{q}_N)]^{\mathsf{T}}$ — nonlin kernel embedding

Can we scale computation with L more gracefully?

- Perhaps, since (9) separable in $l \in \{1, \ldots, L\}$ by construction
- However, explicitly computing $\mathbf{K}$ may be undesirable...

PERK as High-Dimensional Affine Regression

Suppose there exists "approximate feature mapping" $\tilde{\mathbf{z}} : \mathcal{Q} \mapsto \mathbb{R}^Z$ such that $\tilde{\mathbf{Z}} := [\tilde{\mathbf{z}}(\mathbf{q}_1), \ldots, \tilde{\mathbf{z}}(\mathbf{q}_N)]$ has for $\dim(\mathcal{Q}) \ll Z \ll N$

$$\mathbf{K} \approx \tilde{\mathbf{Z}}^\mathsf{T} \tilde{\mathbf{Z}}. \tag{10}$$

PERK as High-Dimensional Affine Regression

Suppose there exists "approximate feature mapping" $\tilde{\mathbf{z}} : \mathcal{Q} \mapsto \mathbb{R}^Z$ such that $\tilde{\mathbf{Z}} := [\tilde{\mathbf{z}}(\mathbf{q}_1), \ldots, \tilde{\mathbf{z}}(\mathbf{q}_N)]$ has for $\dim(\mathcal{Q}) \ll Z \ll N$

$$\mathbf{K} \approx \tilde{\mathbf{Z}}^\mathsf{T} \tilde{\mathbf{Z}}. \tag{10}$$

Plugging (10) into PERK solution (9) and rearranging gives

$$\widehat{x}_l(\cdot) \approx \frac{1}{N} \mathbf{x}_l^\mathsf{T} \mathbf{1}_N + \frac{1}{N} \mathbf{x}_l^\mathsf{T} \mathbf{M} \tilde{\mathbf{Z}}^\mathsf{T} \left(\frac{1}{N} \tilde{\mathbf{Z}} \mathbf{M} \tilde{\mathbf{Z}}^\mathsf{T} + \rho_l \mathbf{I}_Z \right)^{-1} \left(\tilde{\mathbf{z}}(\cdot) - \frac{1}{N} \tilde{\mathbf{Z}} \mathbf{1}_N \right)$$

PERK as High-Dimensional Affine Regression

Suppose there exists "approximate feature mapping" $\tilde{\mathbf{z}} : \mathcal{Q} \mapsto \mathbb{R}^Z$ such that $\tilde{\mathbf{Z}} := [\tilde{\mathbf{z}}(\mathbf{q}_1), \ldots, \tilde{\mathbf{z}}(\mathbf{q}_N)]$ has for $\dim(\mathcal{Q}) \ll Z \ll N$

$$\mathbf{K} \approx \tilde{\mathbf{Z}}^\mathsf{T} \tilde{\mathbf{Z}}. \tag{10}$$

Plugging (10) into PERK solution (9) and rearranging gives

$$\widehat{x}_l(\cdot) \approx \widehat{m}_{x_l} + \widehat{\mathbf{c}}_{x_l\tilde{\mathbf{z}}}^\mathsf{T} \left(\widehat{\mathbf{C}}_{\tilde{\mathbf{z}}\tilde{\mathbf{z}}} + \rho_l \mathbf{I}_Z \right)^{-1} (\tilde{\mathbf{z}}(\cdot) - \widehat{\mathbf{m}}_{\tilde{\mathbf{z}}}) \tag{11}$$

which is regularized Z-dimensional affine regression!

PERK as High-Dimensional Affine Regression

Suppose there exists "approximate feature mapping" $\tilde{\mathbf{z}} : \mathcal{Q} \mapsto \mathbb{R}^Z$ such that $\tilde{\mathbf{Z}} := [\tilde{\mathbf{z}}(\mathbf{q}_1), \ldots, \tilde{\mathbf{z}}(\mathbf{q}_N)]$ has for $\dim(\mathcal{Q}) \ll Z \ll N$

$$\mathbf{K} \approx \tilde{\mathbf{Z}}^\mathsf{T} \tilde{\mathbf{Z}}. \tag{10}$$

Plugging (10) into PERK solution (9) and rearranging gives

$$\widehat{x}_l(\cdot) \approx \widehat{m}_{x_l} + \widehat{\mathbf{c}}_{x_l\tilde{\mathbf{z}}}^\mathsf{T} \left(\widehat{\mathbf{C}}_{\tilde{\mathbf{z}}\tilde{\mathbf{z}}} + \rho_l \mathbf{I}_Z \right)^{-1} (\tilde{\mathbf{z}}(\cdot) - \widehat{\mathbf{m}}_{\tilde{\mathbf{z}}}) \tag{11}$$

which is regularized Z-dimensional affine regression!

Does such a $\tilde{\mathbf{z}}$ exist and work well in practice?

- Yes, *e.g.* for Gaussian $k(\mathbf{q}, \mathbf{q}') \leftarrow \exp\left(-\frac{1}{2} \left\| \mathbf{\Lambda}^{-1} (\mathbf{q} - \mathbf{q}') \right\|_2^2 \right)$
  [Rahimi and Recht, 2007]
- In such cases, can reduce from $\sim N^2$ to $\sim NZ$ computations

Experimental Setup

Demonstrated PERK for T_1, T_2 est from optim (2SP,1DE) scan

Experimental Setup

Demonstrated PERK for T_1, T_2 est from optim (2SP,1DE) scan

- PERK trained using $N \leftarrow 10^5$ samples from prior dist $\mathrm{p}_{\mathbf{x},\boldsymbol{\nu}}$
- To enable precise estimation, support of $\mathrm{p}_{\mathbf{x},\boldsymbol{\nu}}$ carefully chosen to coincide with min-max acquisition design support

Experimental Setup

Demonstrated PERK for T_1, T_2 est from optim (2SP,1DE) scan

- PERK trained using $N \leftarrow 10^5$ samples from prior dist $\mathrm{p}_{\mathbf{x},\boldsymbol{\nu}}$
- To enable precise estimation, support of $\mathrm{p}_{\mathbf{x},\boldsymbol{\nu}}$ carefully chosen to coincide with min-max acquisition design support

Compared PERK to two well-suited ML estimators:

- dictionary-based grid search estimator via variable projection method (VPM) [Golub and Pereyra, 2003]
- local optim estimator via preconditioned variant (PGPM) of classical gradient projection method [Rosen, 1960]

Phantom Results

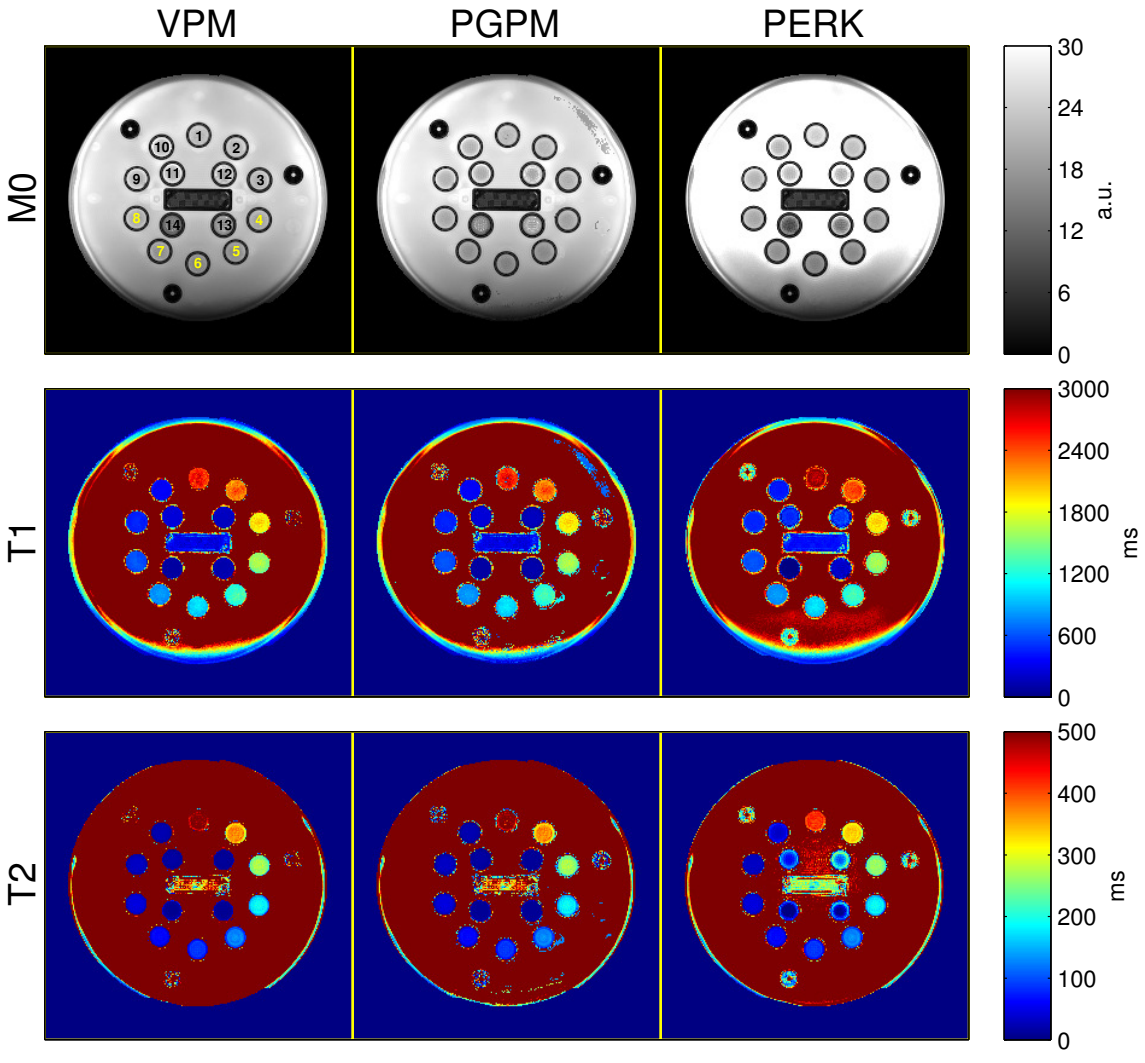

Phantom Results

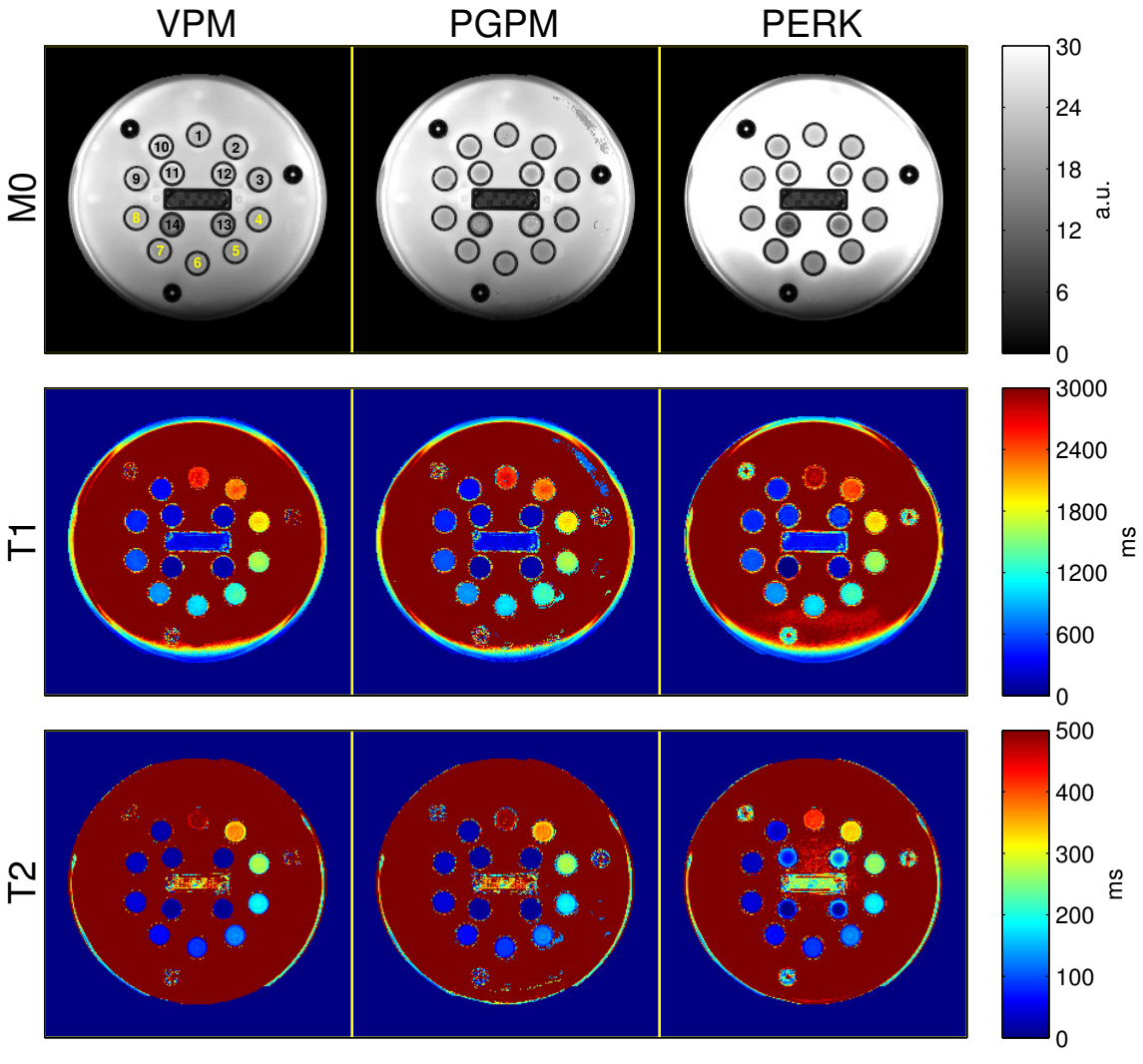

Phantom Results

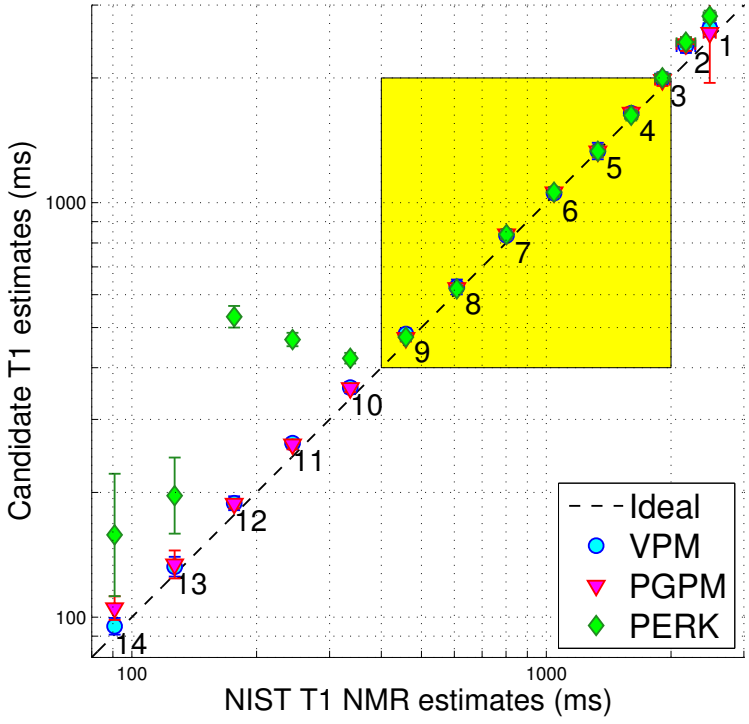

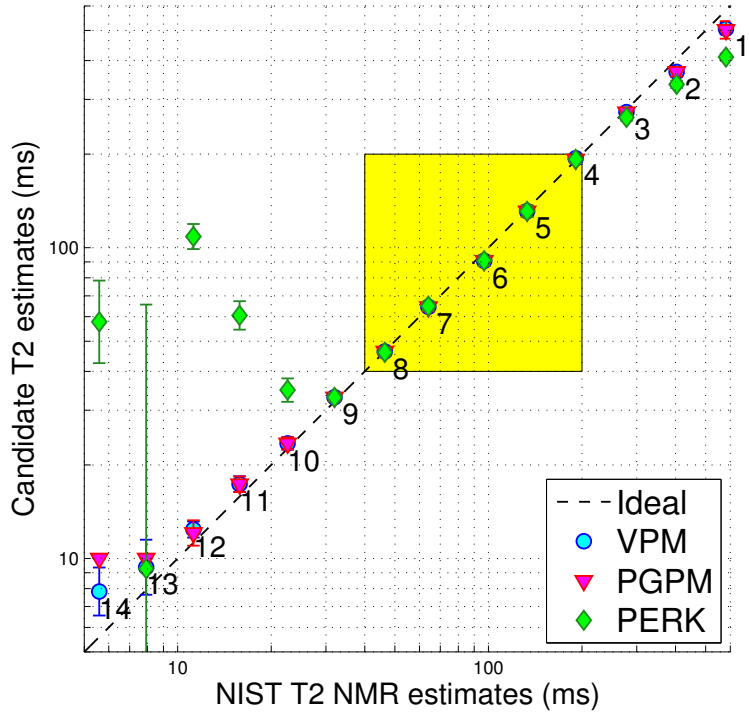

Phantom Results

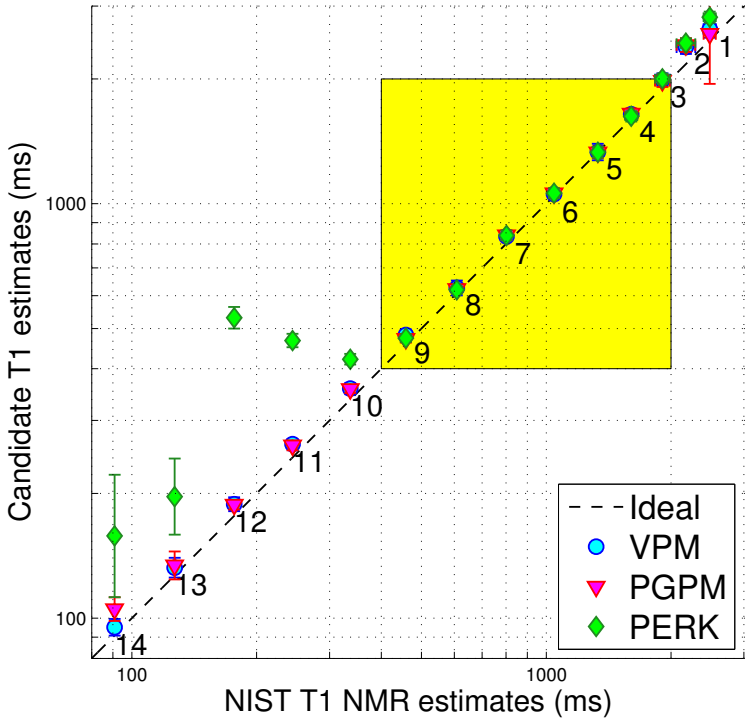

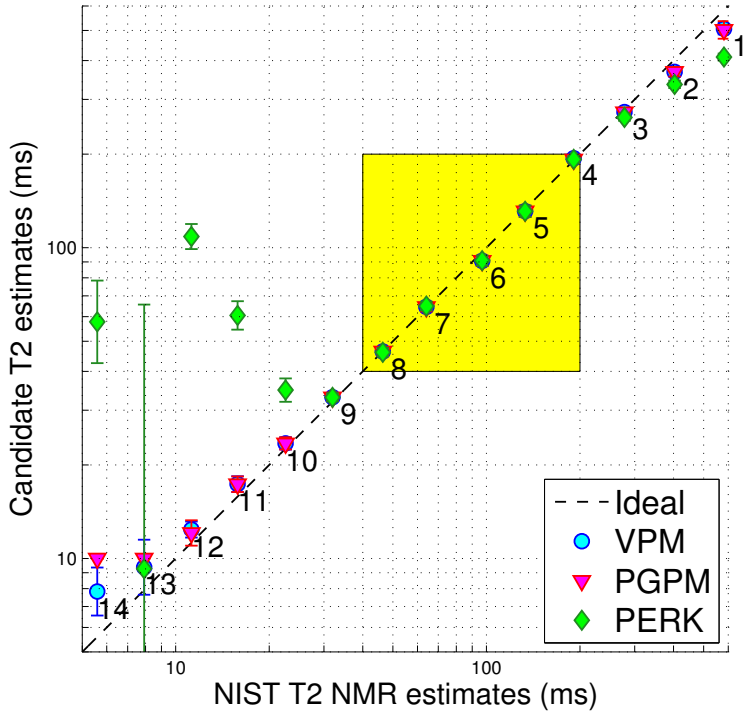

Within support of $p_{\mathbf{x},\boldsymbol{\nu}}$,

PERK and grid search estimates agree excellently.

In vivo Results

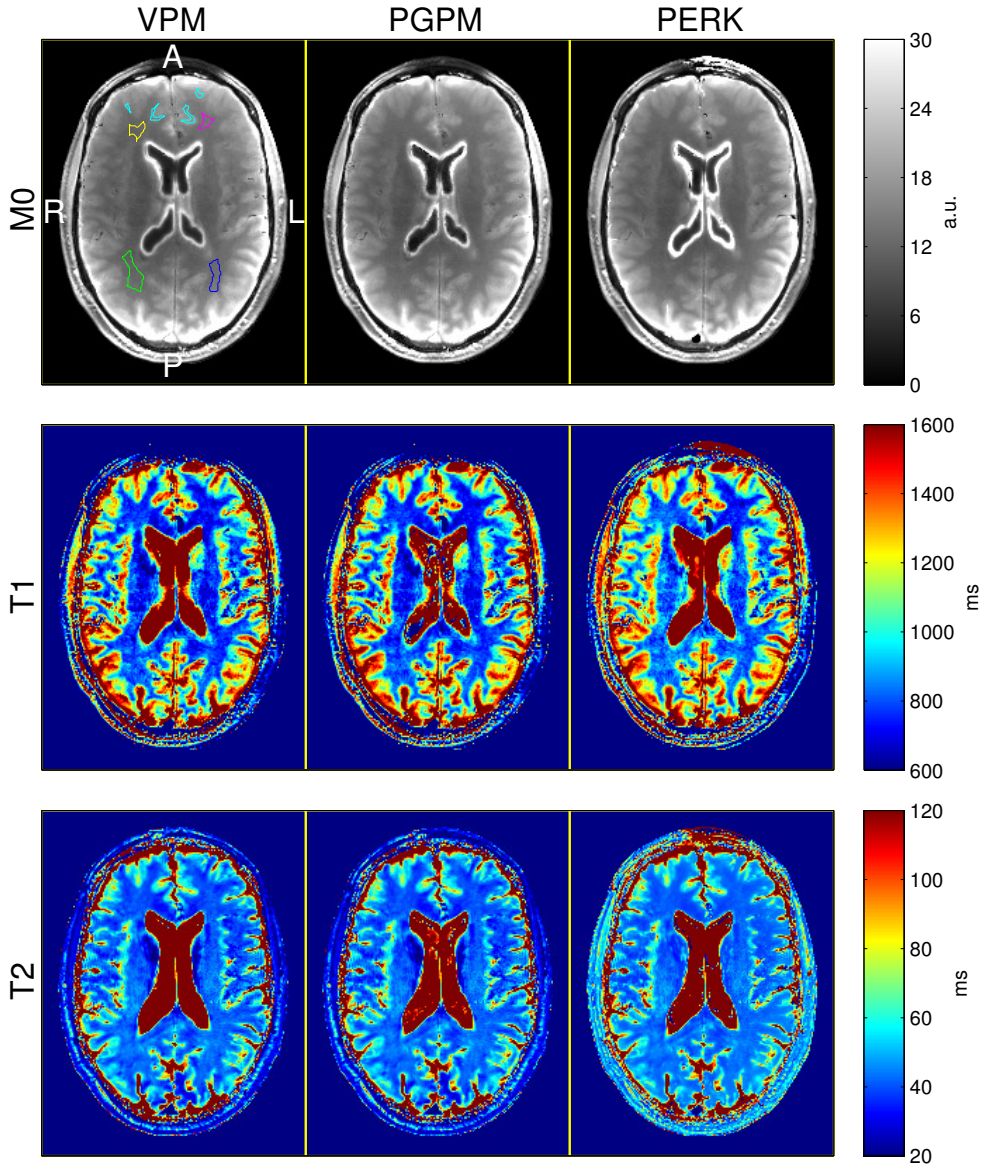

In vivo Results

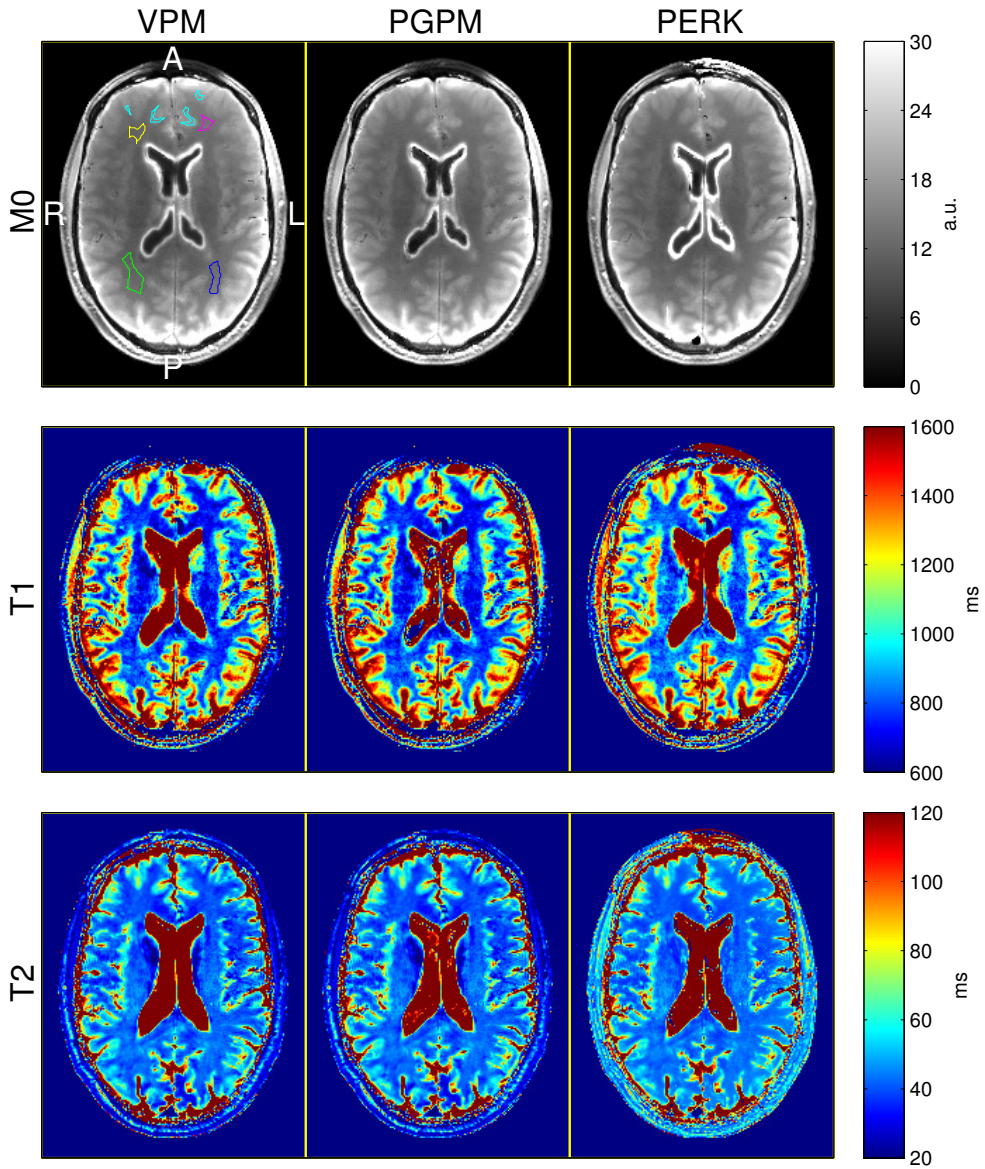

838s 2178s 4.2s train
1.6s test

Summary

Contributions

- **PERK**: fast, dictionary-free estimator for QMRI

Summary

Contributions

- **PERK**: fast, dictionary-free estimator for QMRI
- demonstrated PERK for T_1, T_2 estimation
  - Phantom (and omitted simulation) results show that PERK and ML estimators yield comparable accuracy/precision
  - *In vivo* PERK and ML estimates are comparable in WM/GM
  - **PERK is consistently at least** 140**x faster**

Summary

Contributions

- **PERK**: fast, dictionary-free estimator for QMRI
- demonstrated PERK for T_1, T_2 estimation
  - Phantom (and omitted simulation) results show that PERK and ML estimators yield comparable accuracy/precision
  - *In vivo* PERK and ML estimates are comparable in WM/GM
  - **PERK is consistently at least 140x faster**

Can we exploit PERK's speed in a more compelling problem?

Overview

Advances in Quantitative MRI:

- **Acquisition** [Ch. 4]
  How can we assemble fast, informative collections of scans to enable precise biomarker quantification?
- **Estimation** [Ch. 5]
  Given accurate models and informative data, how can we rapidly quantify these biomarkers?
- **Application** [Ch. 6]
  Using these tools, can we design a state-of-the-art biomarker?

Previous MW imaging acquisitions

Multi-echo spin-echo (**MESE**) [Mackay et al., 1994]

- Considered a gold-standard
- Speed-limited by long repetition times ($\sim$1-2s)

Previous MW imaging acquisitions

Multi-echo spin-echo (**MESE**) [Mackay et al., 1994]

- Considered a gold-standard
- Speed-limited by long repetition times (∼1-2s)

Combinations of fast steady-state scans using variable flip angles ("**mcDESPOT**") [Deoni et al., 2008]

- Whole-brain, high-resolution MW imaging in ∼30m
- Disagree with MESE MWF estimates [Zhang et al., 2015]
  likely due to insufficient precision [Lankford and Does, 2013]

Previous MW imaging acquisitions

Multi-echo spin-echo (**MESE**) [Mackay et al., 1994]

- Considered a gold-standard
- Speed-limited by long repetition times (∼1-2s)

Combinations of fast steady-state scans using variable flip angles ("**mcDESPOT**") [Deoni et al., 2008]

- Whole-brain, high-resolution MW imaging in ∼30m
- Disagree with MESE MWF estimates [Zhang et al., 2015]
  likely due to insufficient precision [Lankford and Does, 2013]

Goal: fast, accurate MW content quantification in WM

A voxel-scale MW content model

simple two-compartment model

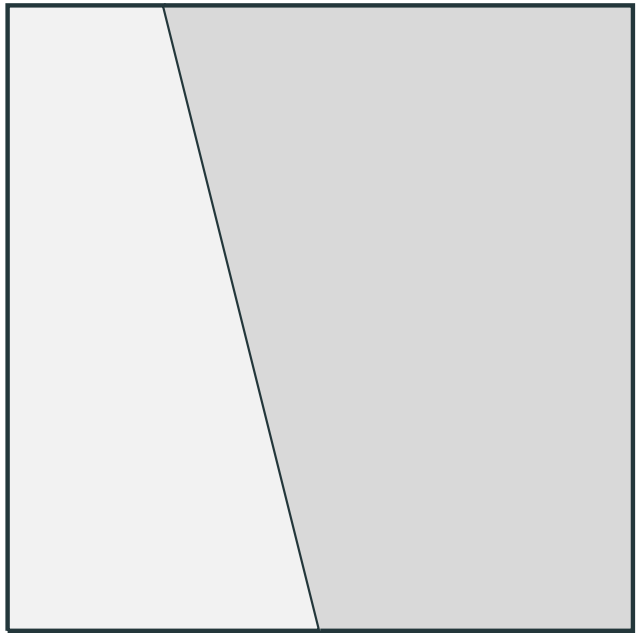

A voxel-scale MW content model

simple two-compartment model

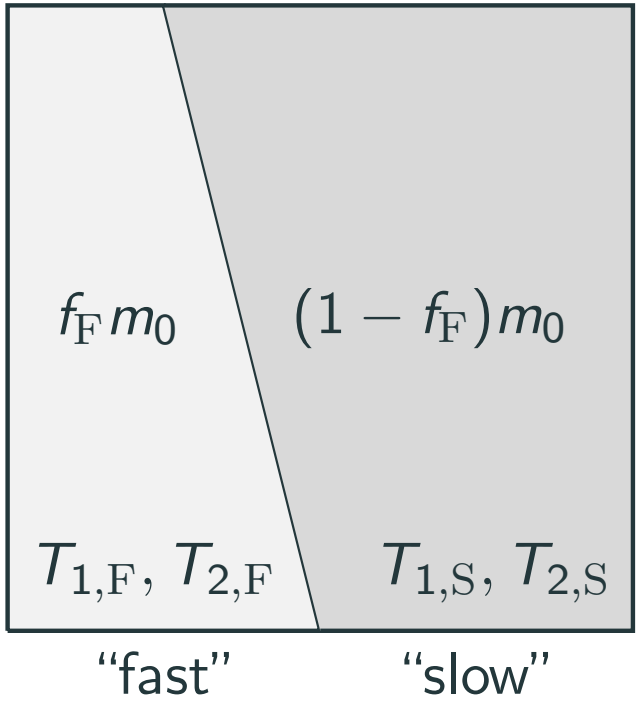

A voxel-scale MW content model

simple two-compartment model

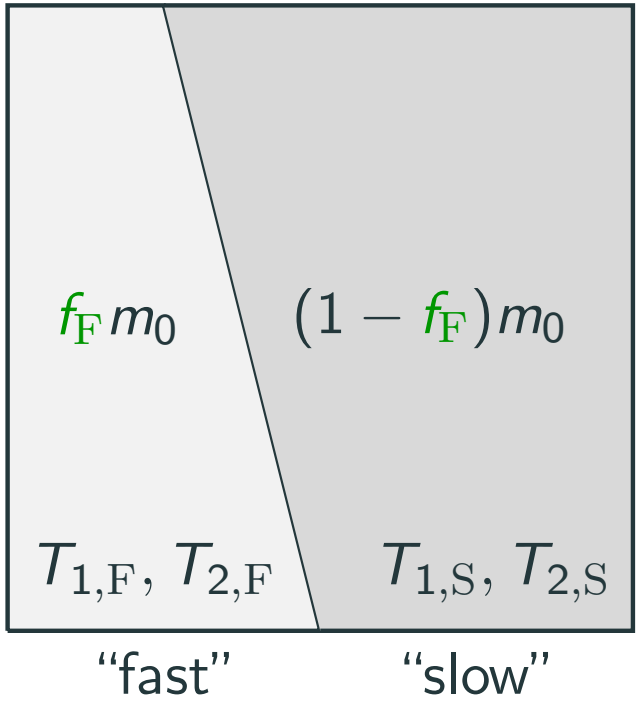

Take fast-relaxing fraction f_F as a simple measure of MW content

Multi-compartmental MR signal models

Two-compartment SPGR model [Spencer and Fishbein, 2000]

- included first-order physical exchange
- neglected relaxation, precession, exchange during excitation

Multi-compartmental MR signal models

Two-compartment SPGR model [Spencer and Fishbein, 2000]

- included first-order physical exchange
- neglected relaxation, precession, exchange during excitation
- absorbing off-resonance effects into m_0 *implies* neglecting exchange between excitation and readout

Multi-compartmental MR signal models

Two-compartment SPGR model [Spencer and Fishbein, 2000]

- included first-order physical exchange
- neglected relaxation, precession, exchange during excitation
- absorbing off-resonance effects into m_0 *implies* neglecting exchange between excitation and readout

Two-compartment DESS model [Nataraj et al., 2017a]

- additional approximations required unless we assume time-independent diff in compartmental off-resonance freq

Multi-compartmental MR signal models

Two-compartment SPGR model [Spencer and Fishbein, 2000]

- included first-order physical exchange
- neglected relaxation, precession, exchange during excitation
- absorbing off-resonance effects into m_0 *implies* neglecting exchange between excitation and readout

Two-compartment DESS model [Nataraj et al., 2017a]

- additional approximations required unless we assume time-independent diff in compartmental off-resonance freq
- including exchange, closed-form solutions still elusive

Multi-compartmental MR signal models

Two-compartment SPGR model [Spencer and Fishbein, 2000]

- included first-order physical exchange
- neglected relaxation, precession, exchange during excitation
- absorbing off-resonance effects into m_0 *implies* neglecting exchange between excitation and readout

Two-compartment DESS model [Nataraj et al., 2017a]

- additional approximations required unless we assume time-independent diff in compartmental off-resonance freq
- including exchange, closed-form solutions still elusive

For simplicity, we use short echo times and neglect exchange.

Bayesian Acquisition Design

$$\check{\mathbf{P}} \in \left\{ \arg \min_{\mathbf{P} \in \mathbb{P}} \bar{\Psi}(\mathbf{P}) \right\}, \text{ where}$$

$$\bar{\Psi}(\mathbf{P}) := \mathsf{E}_{\mathbf{x},\boldsymbol{\nu}} \left(\mathrm{tr} \left(\mathbf{W} \mathbf{F}^{-1}(\mathbf{x}; \boldsymbol{\nu}, \mathbf{P}) \mathbf{W}^{\mathsf{T}} \right) \right) \tag{12}$$

Bayesian Acquisition Design

$$\check{\mathbf{P}} \in \left\{ \arg \min_{\mathbf{P} \in \mathbb{P}} \bar{\Psi}(\mathbf{P}) \right\}, \text{ where}$$

$$\bar{\Psi}(\mathbf{P}) := \mathrm{E}_{\mathbf{x},\boldsymbol{\nu}} \left(\mathrm{tr} \left(\mathbf{W} \mathbf{F}^{-1}(\mathbf{x}; \boldsymbol{\nu}, \mathbf{P}) \mathbf{W}^{\mathsf{T}} \right) \right) \tag{12}$$

- $\mathbf{x}$ $[f_{\mathrm{F}}, T_{1,\mathrm{F}}, T_{2,\mathrm{F}}, T_{1,\mathrm{S}}, T_{2,\mathrm{S}}, m_0]^{\mathsf{T}}$
- $\boldsymbol{\nu}$ transmit field spatial variation s^{t}
- $\mathbf{P}$ SPGR/DESS nominal flip angles, repetition times

Bayesian Acquisition Design

$$\check{\mathbf{P}} \in \left\{ \arg \min_{\mathbf{P} \in \mathbb{P}} \bar{\Psi}(\mathbf{P}) \right\}, \text{ where}$$

$$\bar{\Psi}(\mathbf{P}) := \mathsf{E}_{\mathbf{x},\boldsymbol{\nu}} \left(\mathrm{tr} \left(\mathbf{W} \mathbf{F}^{-1}(\mathbf{x}; \boldsymbol{\nu}, \mathbf{P}) \mathbf{W}^{\mathsf{T}} \right) \right) \tag{12}$$

- $\mathbf{x}$ $[f_{\mathrm{F}}, T_{1,\mathrm{F}}, T_{2,\mathrm{F}}, T_{1,\mathrm{S}}, T_{2,\mathrm{S}}, m_0]^{\mathsf{T}}$
- $\boldsymbol{\nu}$ transmit field spatial variation s^{t}
- $\mathbf{P}$ SPGR/DESS nominal flip angles, repetition times
- $\mathbf{W}$ $\mathrm{diag}\left(\left[(\mathsf{E}_{\mathbf{x},\boldsymbol{\nu}}(f_{\mathrm{F}}))^{-1}, \mathbf{0}_5^{\mathsf{T}} \right]^{\mathsf{T}} \right)$

Bayesian Acquisition Design

$$\check{\mathbf{P}} \in \left\{ \arg \min_{\mathbf{P} \in \mathbb{P}} \bar{\Psi}(\mathbf{P}) \right\}, \text{ where}$$

$$\bar{\Psi}(\mathbf{P}) := \mathrm{E}_{\mathbf{x},\boldsymbol{\nu}} \left(\mathrm{tr} \left(\mathbf{W} \mathbf{F}^{-1}(\mathbf{x}; \boldsymbol{\nu}, \mathbf{P}) \mathbf{W}^{\mathsf{T}} \right) \right) \tag{12}$$

- $\mathbf{x}$ $[f_{\mathrm{F}}, T_{1,\mathrm{F}}, T_{2,\mathrm{F}}, T_{1,\mathrm{S}}, T_{2,\mathrm{S}}, m_0]^{\mathsf{T}}$
- $\boldsymbol{\nu}$ transmit field spatial variation s^{t}
- $\mathbf{P}$ SPGR/DESS nominal flip angles, repetition times
- $\mathbf{W}$ $\mathrm{diag}\left(\left[(\mathrm{E}_{\mathbf{x},\boldsymbol{\nu}}(f_{\mathrm{F}}))^{-1}, \mathbf{0}_5^{\mathsf{T}} \right]^{\mathsf{T}} \right)$
- $\mathrm{E}_{\mathbf{x},\boldsymbol{\nu}}(\cdot)$ approximated via empirical averages of samples drawn from separable prior

Bayesian Acquisition Design

$$\check{\mathbf{P}} \in \left\{ \arg \min_{\mathbf{P} \in \mathbb{P}} \bar{\Psi}(\mathbf{P}) \right\}, \text{ where}$$

$$\bar{\Psi}(\mathbf{P}) := \mathrm{E}_{\mathbf{x},\boldsymbol{\nu}} \left(\mathrm{tr} \left(\mathbf{W} \mathbf{F}^{-1}(\mathbf{x}; \boldsymbol{\nu}, \mathbf{P}) \mathbf{W}^{\mathsf{T}} \right) \right) \tag{12}$$

- $\mathbf{x}$ $[f_{\mathrm{F}}, T_{1,\mathrm{F}}, T_{2,\mathrm{F}}, T_{1,\mathrm{S}}, T_{2,\mathrm{S}}, m_0]^{\mathsf{T}}$
- $\boldsymbol{\nu}$ transmit field spatial variation s^{t}
- $\mathbf{P}$ SPGR/DESS nominal flip angles, repetition times
- $\mathbf{W}$ $\mathrm{diag}\left(\left[(\mathrm{E}_{\mathbf{x},\boldsymbol{\nu}}(f_{\mathrm{F}}))^{-1}, \mathbf{0}_5^{\mathsf{T}} \right]^{\mathsf{T}} \right)$
- $\mathrm{E}_{\mathbf{x},\boldsymbol{\nu}}(\cdot)$ approximated via empirical averages of samples drawn from separable prior
- $\mathbb{P}$ nom flip angle, total scan time constraints

Optimized SPGR/DESS Acquisition

	Optimized flip angles (deg)	Optimized rep. times (ms)
SPGR	–	–
DESS	$33.0, 18.3, 15.1$	$17.5, 30.2, 60.3$

Table 2: Optimized Scan Parameters, $\check{\mathbf{P}}$

- Predicted f_{F} relative standard deviation in WM
  - Optimized SPGR/DESS: $\sqrt{\bar{\Psi}\left(\check{\mathbf{P}}\right)} = 0.425$
  - mcDESPOT: at least 1 [Lankford and Does, 2013]

Simulation Studies

Applied PERK for f_{F} estimation from optimized DESS acquisition

Simulation Studies

Applied PERK for f_{F} estimation from optimized DESS acquisition

- PERK trained using $N \leftarrow 10^6$ samples from prior dist $\mathrm{p}_{\mathbf{x},\boldsymbol{\nu}}$
- To enable precise estimation, $\mathrm{p}_{\mathbf{x},\boldsymbol{\nu}}$ chosen similar to Bayesian scan design sampling dist, but with finite support

Simulation Studies

Applied PERK for f_{F} estimation from optimized DESS acquisition

- PERK trained using $N \leftarrow 10^6$ samples from prior dist $\mathrm{p}_{\mathbf{x},\boldsymbol{\nu}}$
- To enable precise estimation, $\mathrm{p}_{\mathbf{x},\boldsymbol{\nu}}$ chosen similar to Bayesian scan design sampling dist, but with finite support

Compared DESS PERK f_{F} estimates to:

- DESS ML f_{F} estimates
  (via VPM and unrealistically narrow grid search around truth)

Simulation Studies

Applied PERK for f_{F} estimation from optimized DESS acquisition

- PERK trained using $N \leftarrow 10^6$ samples from prior dist $\mathrm{p}_{\mathbf{x},\boldsymbol{\nu}}$
- To enable precise estimation, $\mathrm{p}_{\mathbf{x},\boldsymbol{\nu}}$ chosen similar to Bayesian scan design sampling dist, but with finite support

Compared DESS PERK f_{F} estimates to:

- DESS ML f_{F} estimates
  (via VPM and unrealistically narrow grid search around truth)
- MESE nonnegative least-squares (NNLS) MWF f_{M} estimates
- MESE regularized NNLS (RNNLS) f_{M} estimates

Two-Compartment Simulation without Model Mismatch

Simulated data to arise from **two** water compartments
each with different nominal T_2 values but **same nominal T_1 value**

- DESS f_{F} estimates use known s^{t}
- MESE f_{M} estimates use known s^{t}, bulk T_1

Two-Compartment Simulation without Model Mismatch

Simulated data to arise from **two** water compartments
each with different nominal T_2 values but **same nominal** T_1 **value**

- DESS f_{F} estimates use known s^{t}
- MESE f_{M} estimates use known s^{t}, bulk T_1

Since no model mismatch, f_{F} and f_{M} estimates are comparable

Two-Compartment Simulation Result

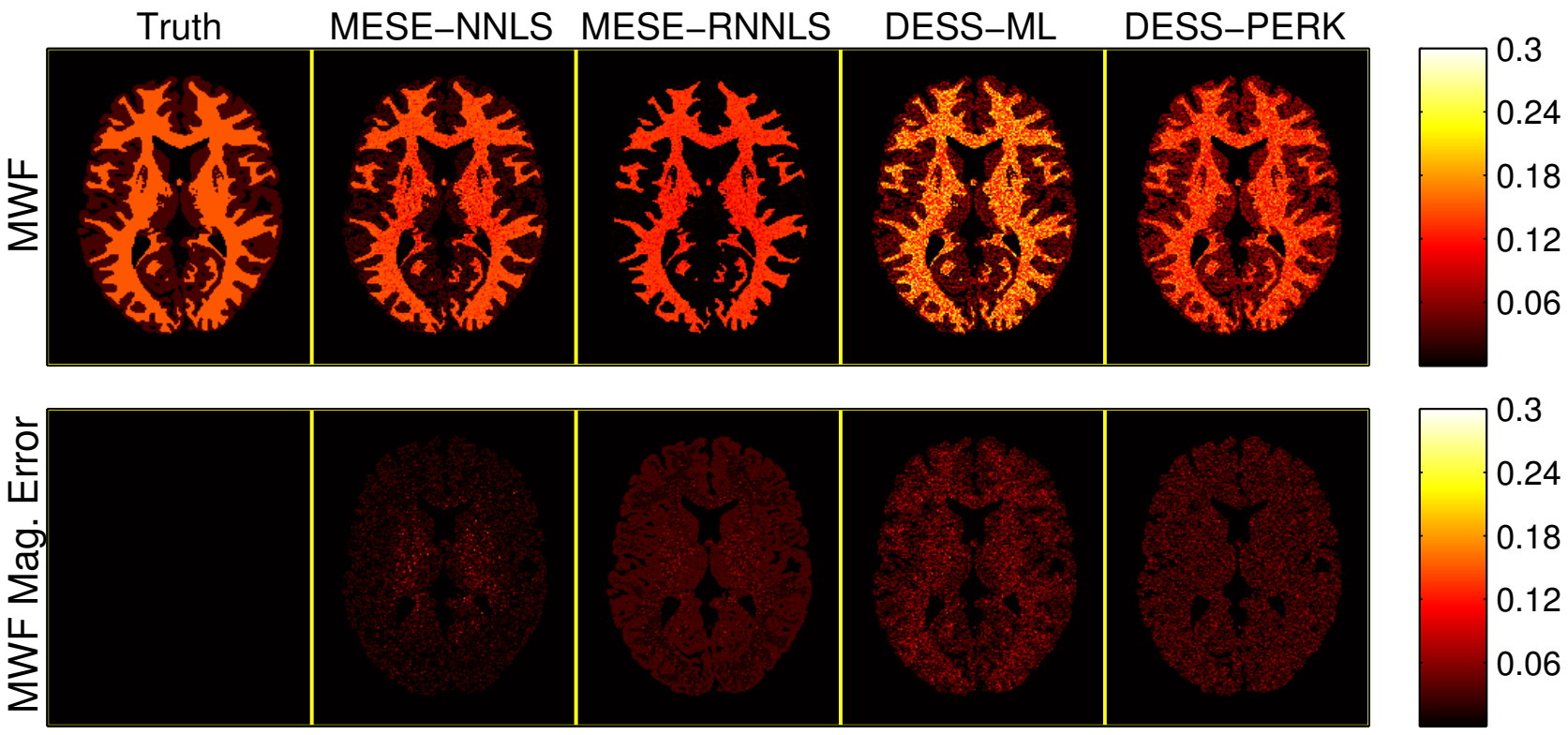

Two-Compartment Simulation Result

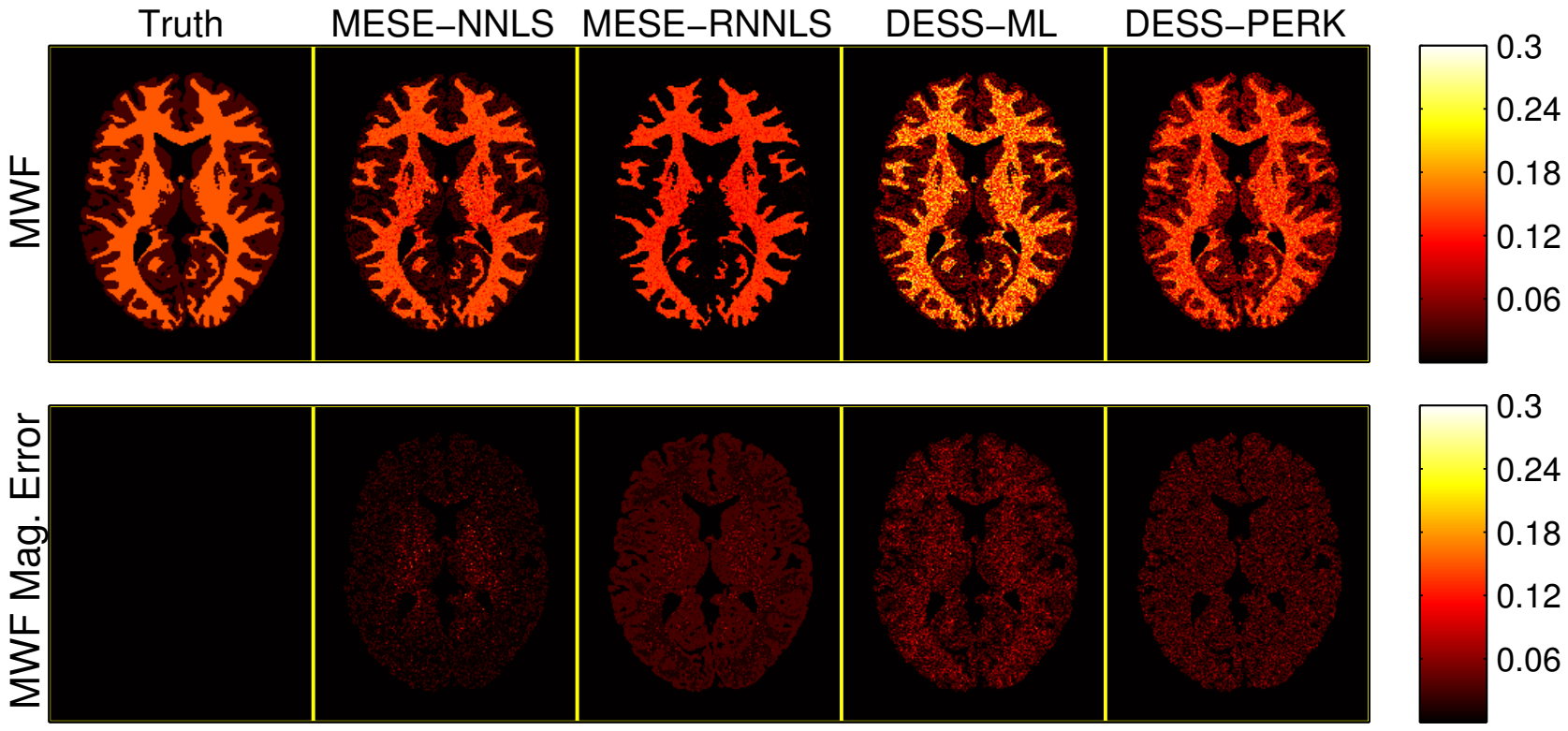

estimation time:		∼5h	33.8s train 1.0s test

Two-Compartment Simulation Result

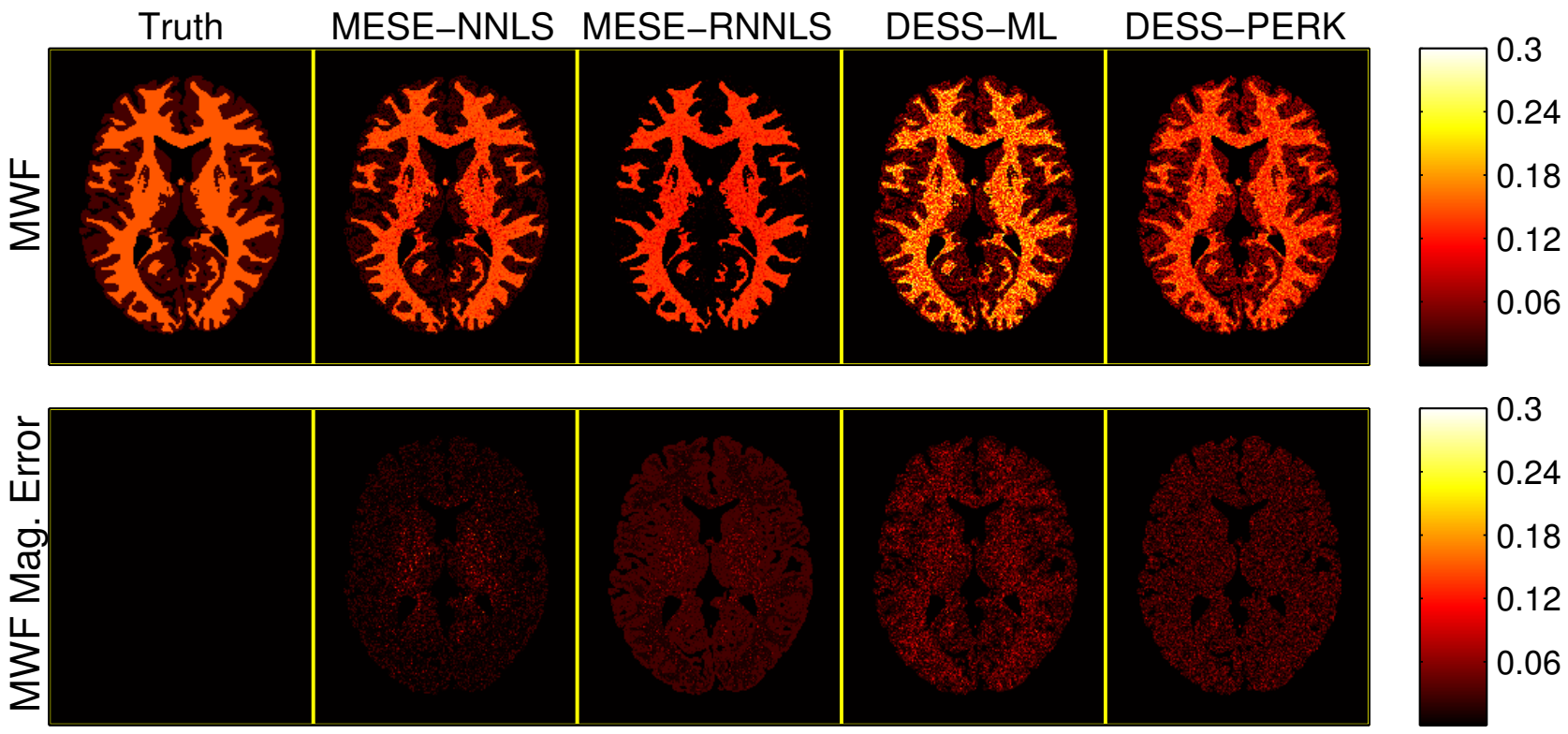

estimation time:			∼5h	33.8s train 1.0s test
WM RMSE:	0.0225	0.0260	0.0433	0.0305

Three-Compartment Simulation with Model Mismatch

Next simulated data to arise from **three** water compartments each with different nominal T_2 **and** T_1 **values**

- DESS f_{F} estimators now incur bias
  due to two-compartment model assumption
- MESE f_{M} estimators now incur bias
  due to bulk-T_1 model assumption (significant for $T_{\mathrm{R}} \sim 1\mathrm{s}$)

Three-Compartment Simulation with Model Mismatch

Next simulated data to arise from **three** water compartments each with different nominal T_2 **and** T_1 **values**

- DESS f_{F} estimators now incur bias
  due to two-compartment model assumption
- MESE f_{M} estimators now incur bias
  due to bulk-T_1 model assumption (significant for $T_{\mathrm{R}} \sim 1\mathrm{s}$)

Due to model mismatch,
f_{F} and f_{M} estimates **need not be comparable**.

Three-Compartment Simulation Result

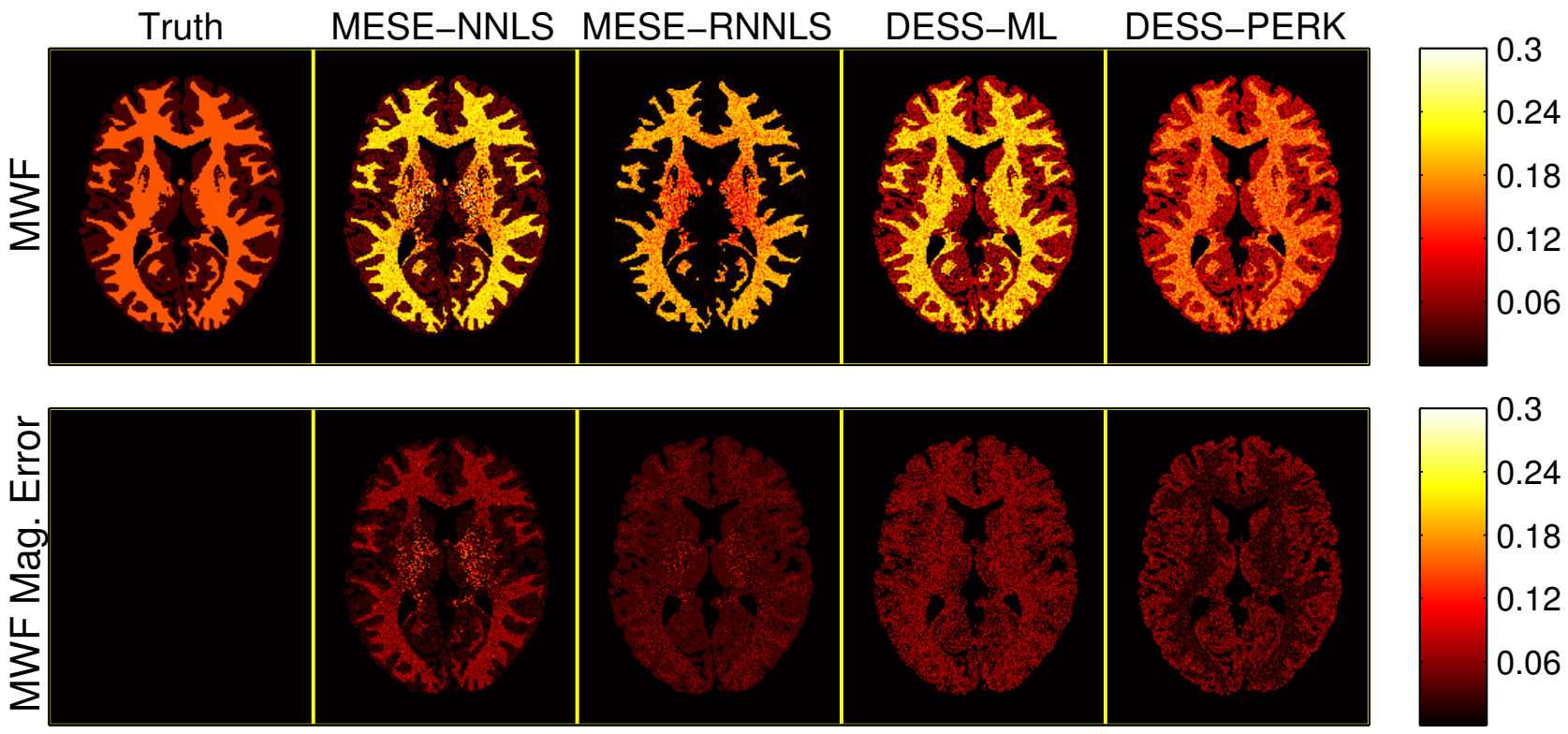

estimation time:		∼5h	34.2s train 1.1s test

Three-Compartment Simulation Result

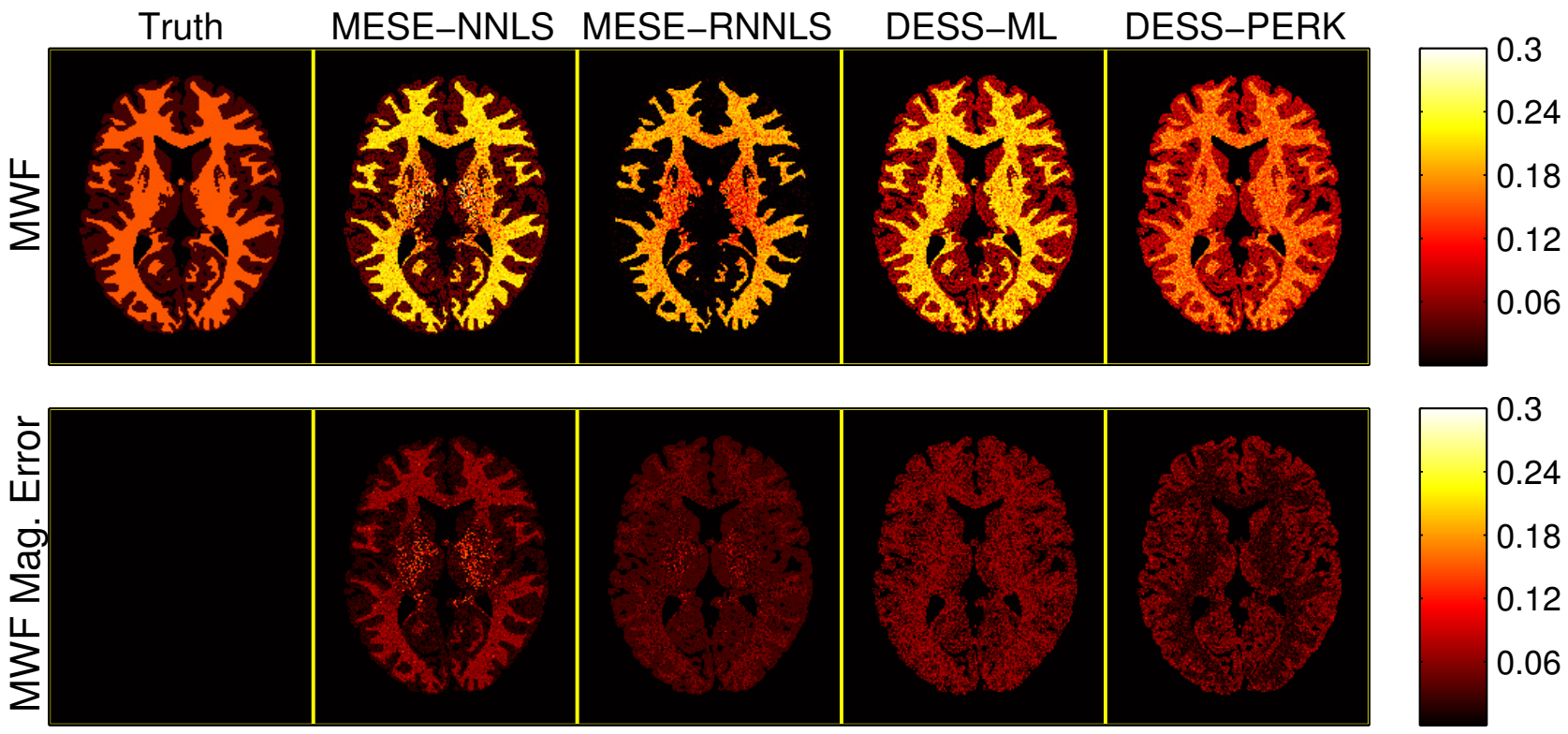

estimation time:			∼5h	34.2s train 1.1s test
WM RMSE:	0.0618	0.0406	0.0559	0.0254

In vivo Experiment

In a single long study of a healthy volunteer:

- Precision-optimized DESS acquisition

In vivo Experiment

In a single long study of a healthy volunteer:

- Precision-optimized DESS acquisition
- 32-echo MESE acquisition
  - Used shaped refocusing pulses
    to suppress out-of-slab signal due to imperfect refocusing
  - Used shorter $T_{\mathrm{R}} \leftarrow 600\mathrm{ms}$ to limit scan time
    (compensated for incomplete recovery w/ separate bulk-T_1 est)
  - Repeated acquisition twice to increase SNR through averaging

In vivo Experiment

In a single long study of a healthy volunteer:

- Precision-optimized DESS acquisition
- 32-echo MESE acquisition
  - Used shaped refocusing pulses
    to suppress out-of-slab signal due to imperfect refocusing
  - Used shorter $T_{\mathrm{R}} \leftarrow 600\mathrm{ms}$ to limit scan time
    (compensated for incomplete recovery w/ separate bulk-T_1 est)
  - Repeated acquisition twice to increase SNR through averaging
- BS acquisition for separate s^{t} estimation
- Variable-flip SPGR acquisition for separate bulk T_1 estimation

In vivo Experiment

In a single long study of a healthy volunteer:

- Precision-optimized DESS acquisition
- 32-echo MESE acquisition
  - Used shaped refocusing pulses
    to suppress out-of-slab signal due to imperfect refocusing
  - Used shorter $T_{\mathrm{R}} \leftarrow 600\mathrm{ms}$ to limit scan time
    (compensated for incomplete recovery w/ separate bulk-T_1 est)
  - Repeated acquisition twice to increase SNR through averaging
- BS acquisition for separate s^{t} estimation
- Variable-flip SPGR acquisition for separate bulk T_1 estimation

Compared DESS PERK f_{F} estimates to:

- MESE NNLS f_{M} estimates
- MESE RNNLS f_{M} estimates

In vivo Results

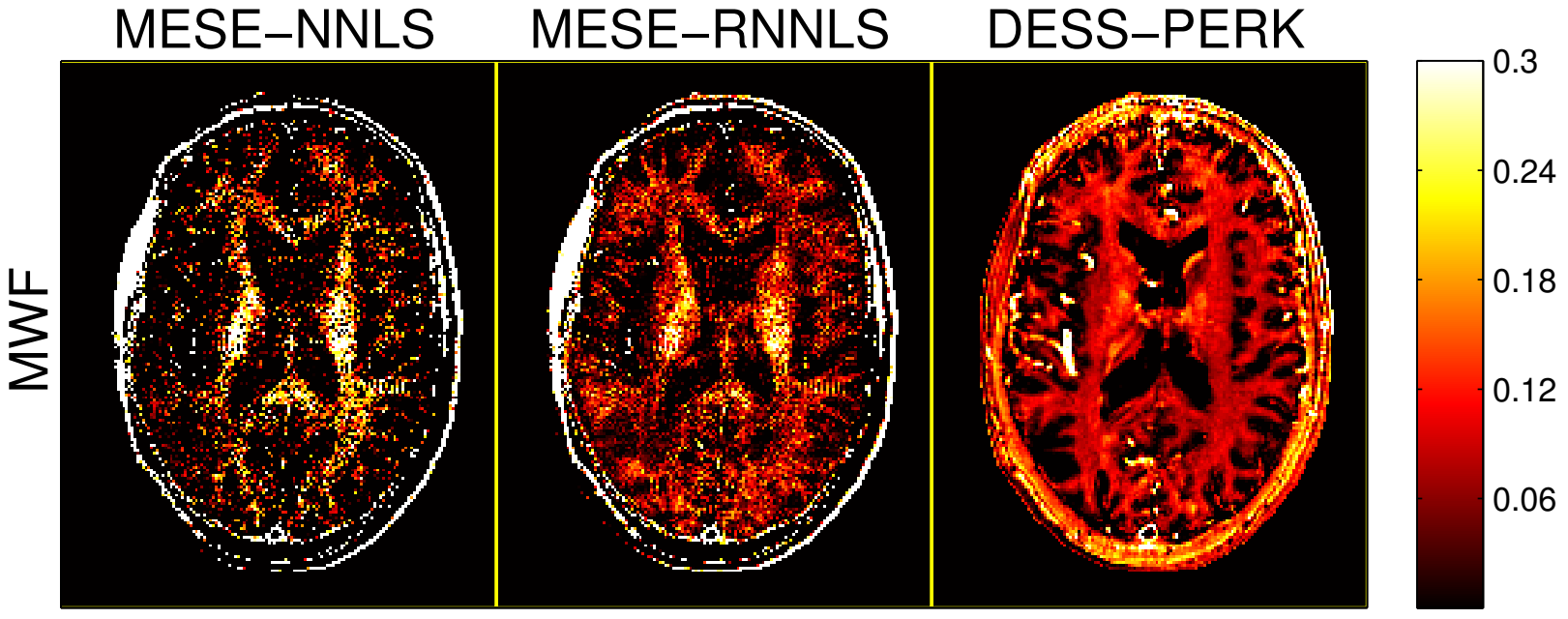

In vivo Results

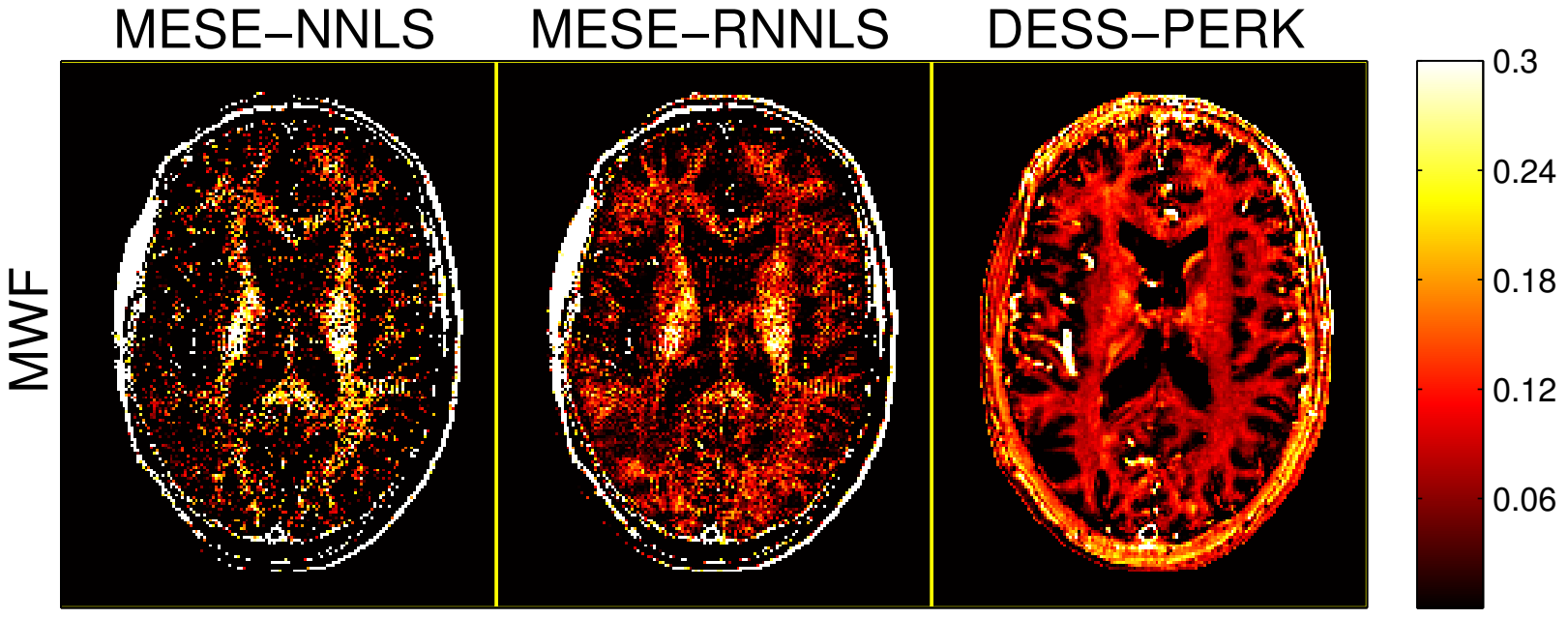

scan time:	40m6s	40m6s	7m45s

Summary

Contribution

- Fast SS MRI acquisition for precise MW imaging

Summary

Contribution

- Fast SS MRI acquisition for precise MW imaging
  - Idealized simulations demonstrate that PERK and ML f_{F} estimates are comparable but PERK is more than 500$\times$ faster.

Summary

Contribution

- Fast SS MRI acquisition for precise MW imaging
  - Idealized simulations demonstrate that PERK and ML f_{F} estimates are comparable but PERK is more than 500$\times$ faster.
  - More realistic simulations demonstrate that both MESE f_{M} and DESS f_{F} estimates are sensitive to model mismatch.

Summary

Contribution

- Fast SS MRI acquisition for precise MW imaging
  - Idealized simulations demonstrate that PERK and ML f_{F} estimates are comparable but PERK is more than 500$\times$ faster.
  - More realistic simulations demonstrate that both MESE f_{M} and DESS f_{F} estimates are sensitive to model mismatch.
  - *In vivo* experiments are the first to demonstrate lateral WM MW content estimates from a SS acquisition that are similar to conventional MESE MWF estimates.

Summary

Contribution

- Fast SS MRI acquisition for precise MW imaging
  - Idealized simulations demonstrate that PERK and ML f_{F} estimates are comparable but PERK is more than 500$\times$ faster.
  - More realistic simulations demonstrate that both MESE f_{M} and DESS f_{F} estimates are sensitive to model mismatch.
  - *In vivo* experiments are the first to demonstrate lateral WM MW content estimates from a SS acquisition that are similar to conventional MESE MWF estimates.

Future Work

- Investigate DESS f_{F} accuracy in *ex vivo* studies
- Correlate with other myelin biomarkers

Summary

Contribution

- Fast SS MRI acquisition for precise MW imaging
  - Idealized simulations demonstrate that PERK and ML f_{F} estimates are comparable but PERK is more than 500$\times$ faster.
  - More realistic simulations demonstrate that both MESE f_{M} and DESS f_{F} estimates are sensitive to model mismatch.
  - *In vivo* experiments are the first to demonstrate lateral WM MW content estimates from a SS acquisition that are similar to conventional MESE MWF estimates.

Future Work

- Investigate DESS f_{F} accuracy in *ex vivo* studies
- Correlate with other myelin biomarkers
- Exploit off-resonance for MW imaging

Summary

Contribution

- Fast SS MRI acquisition for precise MW imaging
  - Idealized simulations demonstrate that PERK and ML f_{F} estimates are comparable but PERK is more than 500$\times$ faster.
  - More realistic simulations demonstrate that both MESE f_{M} and DESS f_{F} estimates are sensitive to model mismatch.
  - *In vivo* experiments are the first to demonstrate lateral WM MW content estimates from a SS acquisition that are similar to conventional MESE MWF estimates.

Future Work

- Investigate DESS f_{F} accuracy in *ex vivo* studies
- Correlate with other myelin biomarkers
- Exploit off-resonance for MW imaging
- Combine PERK with image reconstruction

Numerical Simulation: Acquisition Design

- Simulated many WM-like, GM-like voxel realizations
- Studied sample statistics of T_1, T_2 ML estimates $\widehat{T}_1^{\mathrm{ML}}$, $\widehat{T}_2^{\mathrm{ML}}$

Profile	$(2,1)$	$(1,1)$	$(0,2)$	Truth
WM $\widehat{T}_1^{\mathrm{ML}}$	830 ± 17	830 ± 15	830 ± 14	832
GM $\widehat{T}_1^{\mathrm{ML}}$	$1330 \pm 30.$	1330 ± 24	1330 ± 24	1331
WM $\widehat{T}_2^{\mathrm{ML}}$	$80. \pm 1.0$	$80. \pm 2.1$	79.6 ± 0.94	79.6
GM $\widehat{T}_2^{\mathrm{ML}}$	$110. \pm 1.4$	$110. \pm 3.0$	$110. \pm 1.6$	110

Table 3: $\widehat{T}_1^{\mathrm{ML}}$, $\widehat{T}_2^{\mathrm{ML}}$ sample means $\pm$ sample standard deviations

A Function Space over which Optimization is Tractable

Hilbert space: complete inner product function space

Reproducing kernel Hilbert space (RKHS)

Hilbert space $\mathbb{H}$ over input space $\mathcal{Q}$ with *reproducing property*

$$\langle h, k(\cdot, \mathbf{q}) \rangle_{\mathbb{H}} = h(\mathbf{q}), \qquad \forall h \in \mathbb{H}, \mathbf{q} \in \mathcal{Q}$$

for some $k : \mathcal{Q}^2 \mapsto \mathbb{R}$ called a reproducing kernel (RK)

Relevant facts

- Bijection between RKHS $\mathbb{H}$ and RK k [Aronszajn, 1950]
- Function $k(\cdot, \mathbf{q}) \in \mathbb{H}$ called a *feature mapping*

Function Optimization over a RKHS

Choose: RK $k : \mathcal{Q}^2 \mapsto \mathbb{R}$ that induces choice of RKHS $\mathbb{H}$

Solve: for each desired latent parameter $l \in \{1, \ldots, L\}$,

$$\left(\widehat{h}_l, \widehat{b}_l\right) \in \left\{ \arg \min_{\substack{h_l \in \mathbb{H} \\ b_l \in \mathbb{R}}} \frac{1}{N} \sum_{n=1}^{N} (h_l(\mathbf{q}_n) + b_l - x_{l,n})^2 + \rho_l \|h_l\|_{\mathbb{H}}^2 \right\} \tag{13}$$

- Optimal $\widehat{h}_l$ over $\mathbb{H}$ takes form [Schölkopf et al., 2001]

$$\widehat{h}_l(\cdot) \equiv \sum_{n=1}^{N} \widehat{a}_{l,n} k(\cdot, \mathbf{q}_n) \tag{14}$$

- Plug (14) into (13); solve now instead for $\left(\widehat{a}_l, \widehat{b}_l\right)$; construct:

$$\widehat{x}_l(\cdot) = \sum_{n=1}^{N} \widehat{a}_{l,n} k(\cdot, \mathbf{q}_n) + \widehat{b}_l \tag{15}$$

Numerical Simulation: PERK Estimation

	Truth	VPM	PGPM	PERK
WM T_1	832	832.1 $\pm$ 17.2 (17.2)	832.1 $\pm$ 16.2 (16.2)	833.0 $\pm$ 16.5 (16.5)
GM T_1	1331	1331.5 $\pm$ 31.1 (31.1)	1331.2 $\pm$ 29.7 (29.7)	1332.1 $\pm$ 30.4 (30.4)
WM T_2	79.6	79.61 $\pm$ 0.988 (0.988)	79.60 $\pm$ 0.952 (0.952)	79.46 $\pm$ 0.978 (0.989)
GM T_2	110.	110.02 $\pm$ 1.40 (1.40)	110.02 $\pm$ 1.35 (1.35)	109.91 $\pm$ 1.35 (1.35)

Table 4: Sample means $\pm$ sample standard deviations (RMSEs) of VPM, PGPM, and PERK m_0, T_1, T_2 estimates, computed in simulation over 7810 WM-like and 9162 GM-like voxels.

Mismatch in Scan Design vs. Sampling Dist Support

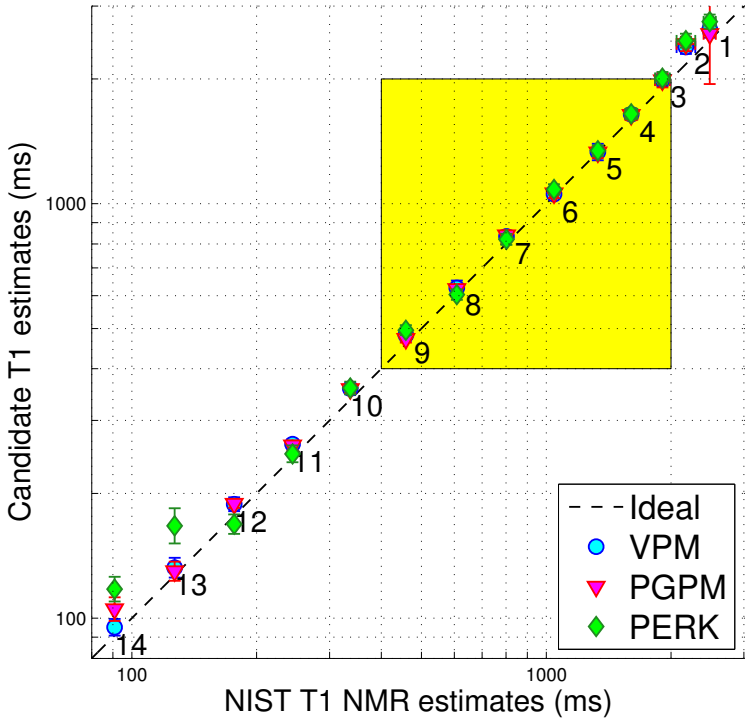

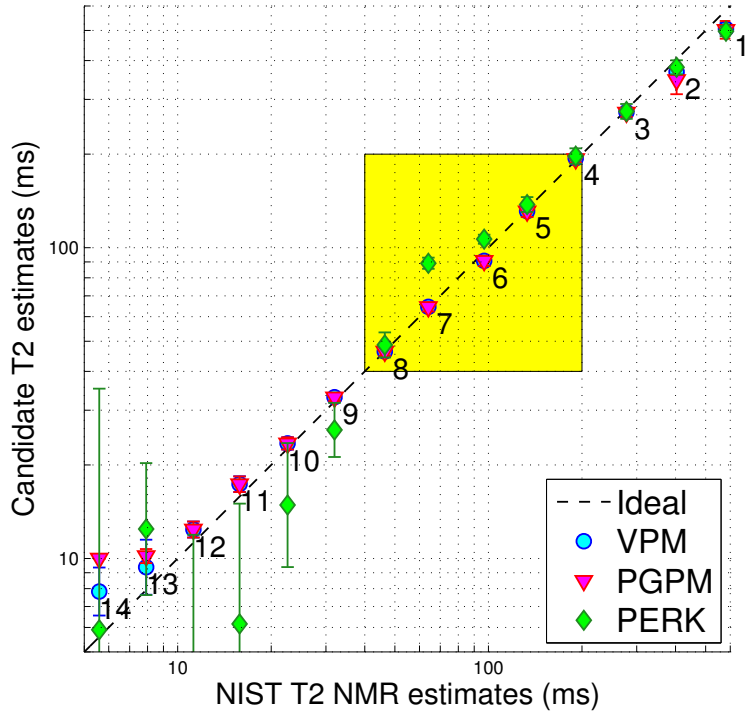

Widening supp($p_{\mathbf{x},\nu}$) degrades performance w/in scan design range.

Thus, scan design and param est should be considered in tandem.

References i


Cramér, H. (1946).
Mathematical methods of statistics.
Princeton Univ. Press, Princeton.


Aronszajn, N. (1950).
Theory of reproducing kernels.
Trans. Amer. Math. Soc., 68(3):337–404.


Bertsimas, D. and Tsitsiklis, J. (1993).
Simulated annealing.
Statistical Science, 8(1):10–15.


Deoni, S. C. L., Rutt, B. K., Arun, T., Pierpaoli, C., and Jones, D. K. (2008).
Gleaning multicomponent T1 and T2 information from steady-state imaging data.
Mag. Res. Med., 60(6):1372–87.

References ii


Golub, G. and Pereyra, V. (2003).
Separable nonlinear least squares: the variable projection method and its applications.
Inverse Prob., 19(2):R1–26.


Hope, M. D., Wrenn, S. J., and Dyverfeldt, P. (2013).
Clinical applications of aortic 4d flow imaging.
Curr. Cardiovasc. Imag. Rep., 6(2):128–39.


Keenan, K. E., Stupic, K. F., Boss, M. A., Russek, S. E., Chenevert, T. L., Prasad, P. V., Reddick, W. E., Cecil, K. M., Zheng, J., Hu, P., and Jackson, E. F. (2016).
Multi-site, multi-vendor comparison of T1 measurement using ISMRM/NIST system phantom.
In *Proc. Intl. Soc. Mag. Res. Med.*, page 3290.

References iii


Lankford, C. L. and Does, M. D. (2013).
On the inherent precision of mcDESPOT.
Mag. Res. Med., 69(1):127–36.


Mackay, A., Whittall, K., Adler, J., Li, D., Paty, D., and Graeb, D. (1994).
In vivo visualization of myelin water in brain by magnetic resonance.
Mag. Res. Med., 31(6):673–7.


Nataraj, G., Nielsen, J.-F., and Fessler, J. A. (2017a).
Myelin water fraction estimation from optimized steady-state sequences using kernel ridge regression.
In *Proc. Intl. Soc. Mag. Res. Med.*, page 5076.


Nataraj, G., Nielsen, J.-F., and Fessler, J. A. (2017b).
Optimizing MR scan design for model-based T1, T2 estimation from steady-state sequences.
IEEE Trans. Med. Imag., 36(2):467–77.

References iv


Nataraj, G., Nielsen, J.-F., Scott, C., and Fessler, J. A. (2018).
Dictionary-free MRI PERK: Parameter estimation via regression with kernels.
IEEE Trans. Med. Imag.
To appear.


Rahimi, A. and Recht, B. (2007).
Random features for large-scale kernel machines.
In *NIPS*.


Redpath, T. W. and Jones, R. A. (1988).
FADE-A new fast imaging sequence.
Mag. Res. Med., 6(2):224–34.


Rosen, J. B. (1960).
The gradient projection method for nonlinear programming, Part I: Linear constraints.
SIAM J. Appl. Math., 8(1):181–217.

References v


Schölkopf, B., Herbrich, R., and Smola, A. J. (2001).
A generalized representer theorem.
In *Proc. Computational Learning Theory (COLT)*, pages 416–426. LNCS 2111.


Spencer, R. G. and Fishbein, K. W. (2000).
Measurement of spin-lattice relaxation times and concentrations in systems with chemical exchange using the one-pulse sequence: breakdown of the Ernst model for partial saturation in nuclear magnetic resonance spectroscopy.
J. Mag. Res., 142(1):120–35.


Zhang, J., Kolind, S. H., Laule, C., and MacKay, A. L. (2015).
Comparison of myelin water fraction from multiecho T2 decay curve and steady-state methods.
Mag. Res. Med., 73(1):223–32.

References vi


Zur, Y., Wood, M. L., and Neuringer, L. J. (1991).
Spoiling of transverse magnetization in steady-state sequences.
Mag. Res. Med., 21(2):251–63.